Plant hydraulic traits regulating productivity and drought resistance in boreal crops

Hui Tang[1,4], Samuli Launianen[2], Julius Vira[1], Liisa Kulmala[1,3], Taru Palosuo[2], Hermanni Aaltonen[1], Olli Nevalainen[1], Istem Fer[1], Henriikka Vekuri[1], Jari-Pekka Nousu[2], Mika Korkiakoski[1], and Jari Liski[1]

[1]Finnish Meteorological Institute (FMI), Climate System Research, Helsinki, Finland
[2]Natural Resources Institute Finland (Luke), Helsinki, Finland
[3]Institute for atmospheric and Earth system research (INAR), University of Helsinki, Finland
[4]Department of Geosciences and Geography, University of Helsinki, Finland

Correspondence: Hui Tang (hui.tang@fmi.fi)

Abstract. Plant hydraulics play a critical role in coordinating photosynthesis, water use, and hydraulic safety when facing water scarcity. The hydraulic traits of boreal crops and their relevance to productivity and drought resistance, however, remain poorly researched. In this study, we combined multi-year carbon and water flux measurements from two Finnish fields representing contrasting boreal cropping systems—a perennial forage grass mixture and an annual cereal crop (oats)—with a novel modelling framework coupling plant photosynthesis, hydraulics, and soil moisture dynamics to decipher the field-level effective hydraulic traits (i.e., apparent hydraulic traits) of the crops and their association with crop performances under varying drought conditions. The model reproduced the observed carbon and water fluxes well and revealed relatively low maximum whole-plant hydraulic conductance and conservative water-use strategies in both crops. Under drought, low hydraulic efficiency prevented soil water depletion and thereby supported high productivity through drought avoidance, whereas its advantage diminished under wetter conditions. Both crops were substantially more susceptible to atmospheric dryness than to soil moisture, highlighting vapor pressure deficit as an important constraint on crop productivity under boreal conditions. The remaining discrepancy between the model-inferred apparent hydraulic traits and available empirical measurements for temperate crops highlights the need for direct hydraulic measurements of boreal crops. Our findings also underscore the importance of incorporating crop hydraulic processes in process-based crop models to gain physiological insights into crop performance and to enhance their accuracy and predictive power under current and future climates.

1 Introduction

Hydraulic traits are plant properties regulating water extraction and transport from the soil to the aerial organs, which play a fundamental role in plant productivity, notably when faced with water scarcity (Cardoso et al., 2025; Torres-Ruiz et al., 2024; Sperry and Love, 2015). Among these traits, two have been most widely studied. One is the maximum hydraulic conductance, which quantifies the efficiency with which water is transported through the whole plant or its individual organs (e.g. roots, stems and leaves) to meet photosynthetic demands (Holloway-Phillips and Brodribb, 2011a; Ocheltree et al., 2016; Gleason et al., 2021). The other is the water potential at which a plant loses 50% of its maximum conductance (ψ_{50}). It is often used

to quantify plant hydraulic safety, i.e. its resistance to drought-induced embolism, loss of water-transport capacity, and the resultant mortality (Choat et al., 2012; Anderegg et al., 2016). These two traits, which characterise, respectively, the hydraulic efficiency and safety of a plant, together play a critical role in shaping the plant's water use strategy.

A trade-off between hydraulic efficiency and safety has been widely documented (Ocheltree et al., 2016; Huo et al., 2022; Zhao et al., 2025), stating that plants capable of efficiently transporting water are often more vulnerable to embolism, and vice versa, because the wider and more interconnected xylem conduits that enable such efficient transport are also more prone to cavitation. An analogous trade-off has also been proposed for stomatal regulation(Henry et al., 2019), whereby maximising stomatal conductance promotes carbon gain but also increases transpirational water loss and the risk of desiccating plant water potential to a damaging level. However, the strength of such a trade-off is still hotly debated (Gleason et al., 2016; Sanchez-Martinez et al., 2020; Liu et al., 2021a), indicating that different species adopt different positions along the efficiency–safety spectrum to improve their fitness under variable environmental conditions. For instance, common crop species (mostly annual cereal crops from temperate and tropical regions) often exhibit high hydraulic conductance (efficiency) but low hydraulic safety (Holloway-Phillips and Brodribb, 2011a; Lamarque et al., 2020; Corso et al., 2020; Canales et al., 2021; Gleason et al., 2021) to obtain high crop productivity, referred to as aquisitive hydraulic strategy. This is particularly the case for annual cereals (Liu et al., 2019). On the other hand, hydraulic traits indicating high safety but low efficiency (i.e., conservative hydraulic strategy) have been widely observed in boreal tree species such as pine and spruce (Li et al., 2023). Perennial crops have been also been known for their conservative hydraulic strategy to survive harsh winters and tolerate more stresses (Vico and Brunsell, 2018; Liu et al., 2019). Although plant hydraulic traits are often considered relatively conserved compared with more plastic plant traits such as photosynthetic capacity (Lamy et al., 2014; Ramírez-Valiente et al., 2025), substantial phenotypical plasticity has also been found in various plants under different conditions (Pritzkow et al., 2020; Sun et al., 2021; Alves et al., 2024; Matzner et al., 2014) and growing stages (Yao et al., 2021). For example, Sun et al. (2021) showed that barley grown under conventional no-tillage management with no tillage exhibited higher hydraulic vulnerability than that under organic farming with intensive tillage.

Despite their significance, it remains elusive how hydraulic traits coordinate in boreal crops and modulate their productivity and drought response. Historically, water limitation has not been a primary concern for humid boreal agroecosystems. Therefore, hydraulic traits and drought tolerance have been less of a priority when selecting or breeding crops for the region, while other traits such as early maturity, cold tolerance, and disease resistance have received more attention (Roitsch et al., 2022). However, the situation has changed in recent years (Poque et al., 2025), as more frequent and severe drought events, characterised by limited soil water availability (soil drought) combined with high atmospheric evaporative demand (atmospheric drought), have been observed and are projected to occur in the future (Spinoni et al., 2018; Rantanen et al., 2023). The hydraulic traits governing the crop response to drought are expected to be under strong selective pressure in the region. Thus, a deeper understanding of the impacts of different types of drought on boreal crops and their association with crop hydraulic traits is urgently needed.

Process-based models with an explicit representation of plant hydraulic processes have emerged only recently and have been shown to better describe plant responses to drought, especially atmospheric drought, than models without hydraulic processes

(Kennedy et al., 2019; Liu et al., 2020; Kubota et al., 2026; Hu et al., 2026). They are also shown to be valuable tools for revealing plant's hydraulic traits through model inversion or calibration (Wang et al., 2020; Gleason et al., 2022; Liu et al., 2021b; Lu et al., 2022). In particular, the use of field-level flux measurements to constrain the hydraulic parameters of such models has been proven effective in retrieving plant hydraulic traits at the field or ecosystem level (Liu et al., 2020). We refer to the average of the hydraulic traits over collective individuals of the same or different species at this scale as "apparent" hydraulic traits, in contrast to the organ- or individual-level hydraulic traits measured on single plants in the laboratory.

In this study, we leverage multi-year observations of carbon and water fluxes from two Finnish crop fields under a perennial forage grass mixture and an annual cereal (oats), respectively. Combining with a novel modelling framework that explicitly couples plant hydraulics, photosynthesis, and soil moisture dynamics, we infer apparent hydraulic traits of the two dominant and contrasting cropping systems in boreal agriculture, and examine their implications for crop functioning at field level. Specifically, our objective is to (i) evaluate the ability of the novel modelling framework to reproduce observed gross primary productivity and evapotranspiration, providing a basis for hydraulic trait inference; (ii) quantify and compare the apparent hydraulic traits of perennial and annual crops and assess their influence on productivity and water-use efficiency; and (iii) determine whether the two cropping systems differ in their resistance to drought and how these differences are associated with their hydraulic traits. In the following, we first describe the modelling framework, study sites and observations, and modelling experiments and workflow for addressing these objectives. We then evaluate the performance of the model, compare inferred hydraulic traits and their effects on crop functioning and drought responses, and finally discuss the broader implications and remaining uncertainties.

2 Materials and Methods

2.1 Structure of SPY-C

We developed a comprehensive soil-plant-atmosphere modelling framework, SPY-C, illustrated in Fig. 1. SPY-C is composed of four interlinked modules mostly from existing models: plant photosynthesis and hydraulics (Phydro), soil water balance (SpaFHy), soil organic carbon decomposition (Yasso), and a simple data-driven phenology and allocation module (PA). SPY-C here stands for **S**paFHy-**P**hydro-**Y**asso for **C**arbon calculation.

2.1.1 Plant hydraulic and photosynthesis module (Phydro)

Phydro is based on Joshi et al. (2022), which unifies plant photosynthesis and hydraulics through a trait-based optimality theory implemented through a single cost-benefit function. The first principle in Phydro is the steady-state leaf water balance, that is, the hydraulic flow rate at which water enters the leaf (the left side of Eq. 1) equals the transpiration rate (the right side of Eq. 1):

$$-\frac{K_p}{\eta}\int_{\psi_{soil}}^{\psi_{soil}-\Delta\psi} P(\psi)\,d\psi = 1.6 g_s D. \tag{1}$$

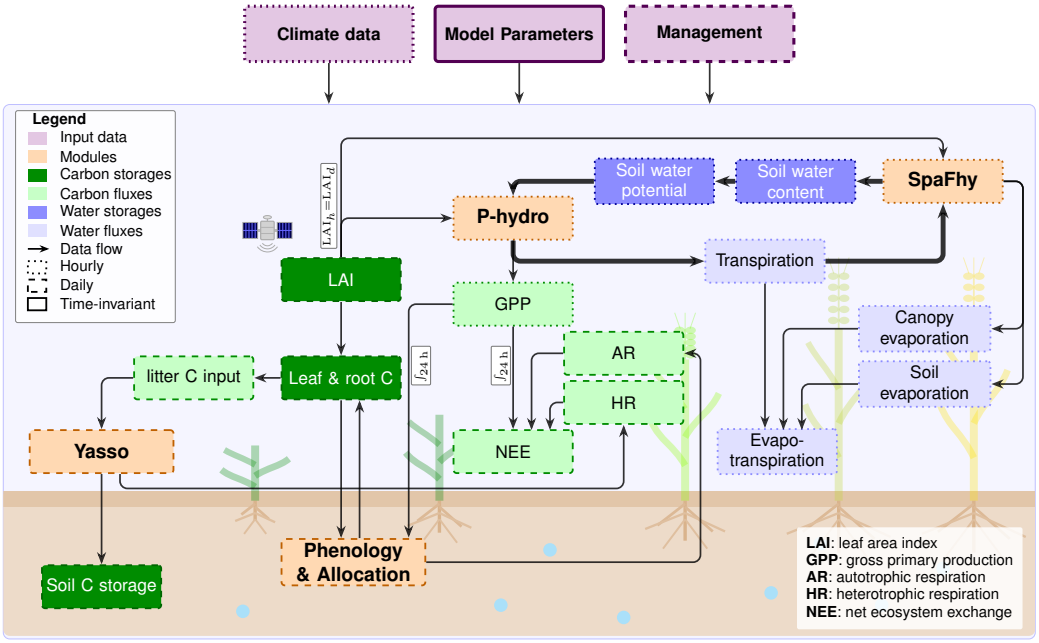

Figure 1. The model structure of SPY-C. Amber and lavender boxes denote model components and input data, respectively. The light and dark green boxes denote carbon fluxes and storages. The light and dark blue boxes denote water fluxes and storages. The outline line style denotes the time step of each module and data stream: dotted = hourly, dashed = daily, and solid = time-invariant. The arrows between boxes denote data flows. The thicker arrows denote the two-way coupling between P-hydro and SpaFhy.

Here, K_p (m) is the maximum whole-plant conductance per unit leaf area, which lumps the entire soil-to-leaf hydraulic pathway (including root, stem, and leaf) into a single effective conductance. η (Pa s) is the dynamic viscosity of water, which is a function of air temperature ($\mathbf{T}$) and pressure ($\mathbf{P_{atm}}$). Note that all the model input variables are denoted by bold. ψ_s (Pa) is the soil water potential. $\Delta\psi$ (Pa) is the difference in water potential between the soil and the leaf (i.e., $\psi_{soil} - \psi_{leaf}$). g_s (mol CO_2 m^{-2} s^{-1}) is the stomatal conductance to CO_2. D is the vapor pressure deficit (**VPD**) divided by $\mathbf{P_{atm}}$. $P(\psi)$ is the vulnerability curve (Eq. 2) that describes the decline in plant water conductance $K(\psi)$ with its water potential (ψ) (Eq. 3):

$$P(\psi) = (1/2)^{(\psi/\psi_{50})^b}, \tag{2}$$

$$K(\psi) = K_p P(\psi), \tag{3}$$

where ψ_{50} is the water potential at which 50% of hydraulic conductivity is lost, and b determines the sensitivity of conductivity loss to water potential. Note that although the hydraulic framework underlying P-hydro was developed primarily in the context of woody plants, its principles are also applicable to grass-like crops, where water is transported through functional xylem

vessels within vascular bundles that provide a continuous hydraulic pathway from roots to leaves, despite the hollow stem structure and absence of secondary woody tissues (Heckwolf et al., 2015).

The second principle is the photosynthetic coordination hypothesis, which states that under typical day time conditions the photosynthetic capacity is optimized so that the carboxylation-limited photosynthesis rate A_c (i.e., the left side of Eq. 4) and light-limited photosynthesis rate A_j (i.e., the right side of Eq. 4) are equal:

$$V_{cmax}\frac{c_i-\Gamma^*}{c_i+K_M}-R_d=\frac{J}{4}\left(\frac{c_i-\Gamma^*}{c_i+2\Gamma^*}\right)-R_d. \tag{4}$$

Here, V_{cmax} (μmol CO_2 m^{-2} s^{-1}) is the maximum carboxylation capacity of leaves. c_i is the leaf-internal CO_2 partial pressure divided by $\mathbf{P_{atm}}$. K_M and Γ^* are the Michaelis-Menten coefficient for C_3 photosynthesis, and the photosynthetic light-compensation point, respectively. Both are a function of $\mathbf{T}$ and $\mathbf{P_{atm}}$. R_d is the dark respiration, which is assumed to be proportional to V_{cmax} (Eq. 5). J (μmol CO_2 m^{-2} s^{-1}) is the effective electron transport capacity of leaves, which is described by Eq. 6. We note that there are still uncertainties on the time scale on which the optimisation of photosynthetic capacity operates, spanning from instantaneous to weekly time scales (Joshi et al., 2022). Here, we assume that the optimization occurs at an hourly time scale to be tightly coupled with soil moisture dynamics during the day, which is also supported by a recent study (Drake et al., 2026).

$$R_d=b_rV_{cmax}, \tag{5}$$

where b_r is a unitless coefficient set to 0.015 in this study (Atkin et al., 2015).

$$J=\frac{4\phi_0 I_{abs}}{\sqrt{\left(\frac{4\phi_0 I_{abs}}{J_{max}}\right)^2+1}}, \tag{6}$$

where ϕ_0 is the intrinsic quantum-yield efficiency, which is a function of $\mathbf{T}$, J_{max} (μmol CO_2 m^{-2} s^{-1}) is the maximum electron transport capacity of leaves under light saturation, I_{abs} ($\mu mol\ s^{-1}m_{leaf}^{-2}$) is the incident photosynthetic photon-flux density per unit leaf area, which is calculated following Eq. 7.

$$I_{abs}=\mathbf{PAR}f_{apar}/\mathbf{LAI}, \tag{7}$$

where $\mathbf{PAR}$ is photosynthetically active radiation ($\mu mol\ m^{-2}s^{-1}$), $\mathbf{LAI}$ (m^2m^{-2}) is the total one-sided green leaf area per unit ground surface area, and f_{apar} is the fraction of absorbed photosynthetically active radiation by the plant, which can be approximated following Beer's law:

$$f_{apar}=1-e^{-k\mathbf{LAI}}, \tag{8}$$

where k is the "effective" canopy light attenuation parameter (including the effect of leaf reflectance and transmittance), which is assumed to be 0.5 in this study. For simplicity, the model does not resolve sunlit/shaded leaf fractions or multiple canopy layers.

The third principle is the steady-state leaf CO_2 balance, which states that the rate of photosynthesis (the left side of Eq. 9, based on Eq. 4), equals the rate at which CO_2 diffuses into the leaves (the right side of Eq. 9):

$$\frac{J}{4} \cdot \frac{c_i(1-b_r) - (\Gamma^* + b_r K_M)}{c_i + 2\Gamma^*} = g_s \mathbf{c_a}(1-\chi). \tag{9}$$

Here, $\mathbf{c_a}$ is the atmospheric CO_2 partial pressure divided by $\mathbf{P_{atm}}$ and χ is the ratio of c_i and $\mathbf{c_a}$.

Furthermore, a cost-benefit function F ($umol\ m^{-2}s^{-1}$) is defined for plants as the benefit of net photosynthetic assimilation (A_j) minus the costs of maintaining the photosynthetic capacity (J_{max}) and the hydraulic pathway ($\Delta\psi$), as given by Eq. 10:

$$F = A_j - \alpha J_{max} - \gamma \Delta\psi^2. \tag{10}$$

Here, α is a unitless coefficient denoting the unit cost of maintaining photosynthetic capacity, such as the regeneration of RuBP and electron transport proteins. γ (μ mol $m^{-2}s^{-1}Pa^{-2}$) denotes the unit cost of maintaining the plant hydraulic pathway, such as the construction cost to build xylem vessels and fibres. Both are conceptual parameters that are inferred rather than directly measured. It is assumed that plants have adapted to their living environment in such a way that they can modulate their stomatal conductance g_s (and thus $\Delta\psi$ according to Eq. 1) and their electron-transport capacity J_{max} independently to maximise their net profit F.

Using Eqs.1-9, the variable A_j in Eq. 10 can be expressed as a function of J_{max} and $\Delta\psi$. As a result, finding the values of J_{max} and $\Delta\psi$ that maximize F becomes a two-dimensional bound-constrained optimisation problem and can be solved using a two-dimensional root finding algorithm (Morales and Nocedal, 2011).

With J_{max} and $\Delta\psi$ being determined, plant gross primary productivity (GPP, μmol CO_2 $m^{-2}s^{-1}$) and transpiration (Tr, μmol H_2O $m^{-2}s^{-1}$) can be calculated according to Eq. 11 and 12:

$$GPP = (A_j + R_d) \cdot LAI, \tag{11}$$

$$Tr = 1.6 g_s D \cdot LAI, \tag{12}$$

where factor 1.6 accounts for the relative diffusivity of water vapor to that of CO_2. V_{cmax}, R_d, and g_s can also be derived according to Eq. 4, 5, and 1, respectively, once J_{max} and $\Delta\psi$ are determined.

2.1.2 Soil water balance module SpaFHy

The soil water balance in SPY-C describes the processes such as infiltration, drainage, and evapotranspiration (ET), the latter consisting of plant transpiration (Eq. 12) and soil evaporation. We adopted representations of rainfall interception, snow accumulation and melt, and a single-layer soil water balance from the SpaFHy (Spatial Forest Hydrology, Launiainen et al., 2019) model. The hydrological processes can be simulated at hourly resolution to enable close coupling with Phydro. The simulated volumetric soil water content is converted to soil water potential using the van Genuchten soil water retention function (Schaap

and Van Genuchten, 2006) and passed to Phydro as an input variable (Fig. 1 and Eq. 13):

$$\psi_{soil} = -\frac{1}{\alpha_v}(S_e^{-\frac{1}{m}} - 1)^{\frac{1}{n}}, \tag{13}$$

where ψ_{soil} (kPa) is the soil water matric potential and α_v, n, and m are empirical shape parameters. The parameter m is commonly expressed as $m = 1 - \frac{1}{n}$. S_e is the effective saturation as given by Eq. 14:

$$S_e = \frac{\theta - \theta_r}{\theta_s - \theta_r}, \tag{14}$$

where θ is the volumetric soil water content (m^3/m^{-3}), θ_s is the saturated soil water content, and θ_r is the residual water content.

To be consistent, the soil hydraulic conductivity (K_{soil}) affecting drainage is also derived using the van Genuchten model (Schaap and Van Genuchten, 2006), which can be written as:

$$K_{soil} = K_{sat} S_e^{0.5}(1 - (1 - S_e^{1/m})^m)^2. \tag{15}$$

Here, K_{sat} $(m\ s^{-1})$ is the saturated hydraulic conductivity. When soil water potential is above field capacity, free drainage according to K_{soil} can occur at the lower boundary of the soil in SpaFhy. There is no explicit estimation of root water potential. Root water conductance has also been lumped into whole-plant hydraulic conductance (K_p) in Phydro. Root water uptake from soil is merely the transpiration demand given by Phydro met from the total soil water storage simulated in SpaFhy. The calculation of canopy interception evaporation and soil evaporation follow the SpaFHy formulations, using Penman-Monteith equation and soil-water availability restricted Priestley-Taylor approach, respectively. Total ET is the sum of canopy and soil evaporation given by SpaFhy, and transpiration flux given by Phydro (Fig. 1).

2.1.3 Phenology and allocation module

The phenology and carbon allocation module (PA) directly allocates daily assimilated carbon ($\overline{GPP}$) into above- (i.e., leaf) and below-ground (i.e., root) carbon pools according to specific allometric ratios, following the concept from Sierra et al. (2022) (Eq. 16 and 17).

$$CF_{gpp:leaf} = \overline{GPP} \cdot a_{leaf}, \tag{16}$$

$$CF_{gpp:root} = \overline{GPP} \cdot a_{root}, \tag{17}$$

where $\overline{GPP}$ denotes the daily accumulation of hourly GPP flux derived by Eq. 11, $CF_{gpp:leaf}$ and $CF_{gpp:root}$ $(umol\ m^{-2}d^{-1})$ are the carbon fluxes from $\overline{GPP}$ to leaf and root, and a_{leaf} and a_{root} are the respective proportions of $\overline{GPP}$ allocated to leaf and root carbon storage at each daily time step. For cereal crops, grains can constitute a significant proportion of the aboveground biomass. The grain filling flux ($CF_{gpp:grain}$) is thus considered and described following Eq. 18:

$$CF_{gpp:grain} = \overline{GPP} \cdot a_{grain}, \tag{18}$$

where a_{grain} denotes the proportion of $\overline{GPP}$ allocated to grain carbon pool at each daily time step. The details on how a_{leaf}, a_{root}, and a_{grain} are derived and constrained by observation can be found in Methods S1 in the Supporting Information (SI).

The newly allocated carbon is then subject to autotrophic respiration (AR), consisting of growth ($CF_{gr,leaf}$, $CF_{gr,root}$, $CF_{gr,grain}$) and maintenance respiration ($CF_{mr,leaf}$, $CF_{mr,root}$, $CF_{mr,grain}$) of the plant organs. In addition, it is assumed that both leaf and root lose their carbon through turnover ($CF_{leaf:litter}$, $CF_{root:litter}$), which produces litter carbon input to soil (Fig. 1). More detailed formulation of these fluxes can also be found in Methods S1.

The changes in carbon storage of leaf (ΔCS_{leaf}), root (ΔCS_{root}), and grain (ΔCS_{grain}) at each time step are given by Eq. 19–20–21, respectively:

$$\Delta CS_{leaf} = CF_{gpp:leaf} - CF_{leaf:litter} - CF_{mr,leaf} - CF_{gr,leaf}, \tag{19}$$

$$\Delta CS_{root} = CF_{gpp:root} - CF_{root:litter} - CF_{mr,root} - CF_{gr,root}, \tag{20}$$

$$\Delta CS_{grain} = CF_{gpp:grain} - CF_{mr,grain} - CF_{gr,grain}. \tag{21}$$

Note that root carbon is tracked as a prognostic pool (Eq. 20) subject to allocation, respiration, and turnover, and it supplies litter to soil decomposition model YASSO. However, this root carbon does NOT dynamically change rooting depth or hydraulic traits: the root-zone depth (0.6 m) and K_p are fixed within a simulation, hence is decoupled from the water/hydraulic routine in the model.

In the current model version, phenology is prescribed rather than dynamically simulated: the seasonal canopy development is imposed through the daily LAI interpolated from Sentinel-2 product (Fig. 2c,d), and reported management events (e.g., harvest, grazing, fertilisation).

2.1.4 Soil decomposition module YASSO

We describe soil carbon balance dynamics and heterotrophic respiration (HR) using a daily timestep version of YASSO20 soil carbon model (Viskari et al., 2022; Heimsch et al., 2024). The litter input ($CF_{leaf:litter}$, $CF_{root:litter}$) is provided by the PA module (Eq. S8 and S9) and the litter quality (i.e., carbon fractions) is prescribed depending on crop types following the study by Palosuo et al. (2015).

Combining the HR derived from YASSO with the autotrophic respiration flux (AR) calculated by the PA module (Eq. S7) sum up to the total ecosystem respiration ($RECO$):

$$RECO = AR + HR. \tag{22}$$

Further, combining $\overline{GPP}$, the net ecosystem exchange (NEE) at a daily time step (Fig. 1) can be expressed as:

$$NEE = RECO - \overline{GPP}. \tag{23}$$

2.1.5 Coupling between model components

As shown in Fig. 1, SPY-C runs on two nested time steps. Phydro and SpaFHy are integrated hourly and two-way coupled: each hour, SpaFHy's soil moisture is converted to soil water potential before passing to Phydro; Phydro solves stomatal conductance and thus transpiration (Eq. 12); the transpiration is then sent to SpaFhy and is withdrawn from the soil water store together with soil evaporation, updating soil moisture for the next hour. The PA and YASSO modules run daily: hourly GPP is accumulated to a daily total, allocated by PA to leaf, root, and grain pools (Eqs. 16-18), and the resulting litter drives YASSO, yielding RECO and NEE on daily scale (Eqs. 22–23). The hourly to daily link is GPP accumulation, while the daily to hourly link is the prescribed canopy state (i.e., LAI). Daily leaf area growth enters the hourly P-hydro calculations through absorbed PAR (Eqs. 7-8) and is used to scale GPP and transpiration to the canopy level (Eqs. 11–12). It modulates both carbon and water fluxes every hour as an observation-driven boundary condition (Fig. 1), rather than as a prognostic variable linked to primary productivity and soil moisture. Consequently, two-way coupling between PA and P-hydro/SpaFhy is not yet fully implemented in the current version of SPY-C.

2.2 Model experiments

2.2.1 Study sites and observation data

Two agricultural fields on mineral (i.e., non-peat) soils in Southern Finland were used in this study (Fig. 2a). The sites were selected to represent two agronomically important and contrasting boreal cropping systems: a perennial forage grass mixture and an annual cereal crop. They differ in crop life form, soil texture, and management, and both are equipped with multi-year eddy covariance flux measurements that support model evaluation and inversion. The Qvidja site (60.29550 °N, 22.39281°E; elevation 5 m) is on the southwestern coast of Finland, which has continuous eddy covariance (EC) flux measurements since May 2018 (Heimsch et al., 2021). During the study period, the footprint area of the flux measurement was covered by a mixture of perennial grasses and legume, dominated by timothy (*Phleum pratense*) and meadow fescue (*Festuca pratensis*). The soil is a relatively fine textured clay loam. The Hauho site (61.13977 °N, 24.58401°E; elevation 89.5 m) has continuous EC measurements since June 2022 (Vira et al., 2025). The footprint area of the flux measurement was primarily covered by oats (*Avena sativa*); in 2023, Italian ryegrass (*Lolium multiforum*) was additionally sown as a cover crop during the growing season. Unlike Qvidja, Hauho has a coarser-textured silty loam soil. Together, these contrasting sites provide a useful test of the model across different crop types and growing conditions and allow us to examine whether field-scale hydraulic traits and water-use strategies differ between perennial and annual boreal cropping systems.

The EC instrumentation at both sites was the same, measuring CO_2/H_2O mixing ratio (LI-7200, LI-COR Biosciences, USA), and three-dimensional wind at 10 Hz frequency (u-Sonic3 Scientific, METEK GmbH, Germany). Besides flux measurements, auxiliary meteorological measurements close to the EC tower were also performed, such as air temperature and relative humidity (Humicap HMP155, Vaisala Oyj, Finland), photosynthetically active radiation, soil temperature (-5 or -10 cm; Pt100 IKES sensors, Nokeval Oy, Finland), and soil moisture (-5 or -10 cm; ML3 ThetaProbe sensor, Delta-T Devices Ltd., UK). The half-hourly turbulent CO_2/H_2O fluxes were calculated using the Eddypro software (v. 7.0.9, LI-COR Bio-

sciences, USA), following standard quality control and filtering protocols (Vira et al., 2025). The gap-filling of the flux data was performed using the method developed by Vekuri et al. (2023). As environmental drivers in the gap-filling, we used air and soil temperature, photosynthetically active radiation, soil moisture, and VPD for both sites, and for the Qvidja site also LAI and precipitation. NEE was partitioned into GPP and RECO. RECO was assumed to follow an Arrhenius-type temperature response function (Lloyd and Taylor, 1994) and parameters were fitted following Reichstein et al. (2005). Parametrization of GPP was based on a nonlinear radiation response function as in Gerin et al. (2023). Both sites experienced drought events of various severity during the observation periods (Fig. 2e,f). For more detailed information about the sites and data, we refer to the aforementioned references, as well as the Field Observatory (https://fieldobservatory.org), which is an open platform for real-time monitoring of crop fields in Finland (Nevalainen et al., 2022a).

2.2.2 Model initialization

All input data required to initialize SPY-C are summarised in Methods S2. Specifically, the meteorological forcing data for the two sites were retrieved from ERA5-Land reanalysis data (Muñoz-Sabater et al., 2021) using their geographical locations. ERA5-Land was used because it provides a gap-free and internally consistent set of all meteorological drivers required by SPY-C over the entire simulation period. Its use also facilitates the transferability of the modelling framework to sites and periods without complete in-situ meteorological observations, which is important for its intended application in the future. ERA5-Land showed good agreement with the on-site measurements for the key meteorological variables at our study sites, such as air temperature, precipitation, and VPD (data not shown).

The annual LAI cycle was prescribed by interpolating the LAI extracted from Sentinel-2 remote sensing products to daily values (Fig. 2c) using a Gaussian process regression as described in Vira et al. (2025). The retrieval of LAI was based on Sentinel-2 level-2A (bottom-of-atmosphere reflectance) products and follows the LAI algorithm (v1.1) developed by Weiss et al. (2020) for the European Space Agency's SNAP software (Science Toolbox Exploitation Platform) and implemented in the satellitetools Python package (https://doi.org/10.5281/zenodo.5993291). The retrieval provides total single-sided green LAI at 20×20 m, which was then aggregated over the EC flux footprint at each site to obtain a field-level total LAI used to drive the model. This aggregation is consistent with the model's big-leaf canopy representation and with the spatial scale at which modelled fluxes were compared with EC observations. Gaussian process regression was used for temporal interpolation of satellite-derived LAI because it can accommodate irregularly spaced observations while providing both a smooth interpolation and an explicit estimate of prediction uncertainty. In the presence of data gaps, the interpolation gradually approaches the mean of the Gaussian process, which was set to zero. This approach was found to perform well under Finnish conditions (Vira et al., 2025), since extended data gaps were almost exclusively during winter, when the fields were snow-covered and LAI was effectively zero. These gaps are reflected in the larger prediction uncertainty of the interpolated time series.

All model parameters used in SPY-C and their values for the two study fields are listed in Table S2. Most parameters were kept at their default values and were identical between sites, except for the soil hydraulic parameters in SpaFhy, which were adjusted to represent site-specific soil texture, and the plant hydraulic parameters in P-hydro, which were calibrated for each crop type (see 2.2.3). The soil depth for root water uptake is set to 0.6 m, which was found to represent available root-zone

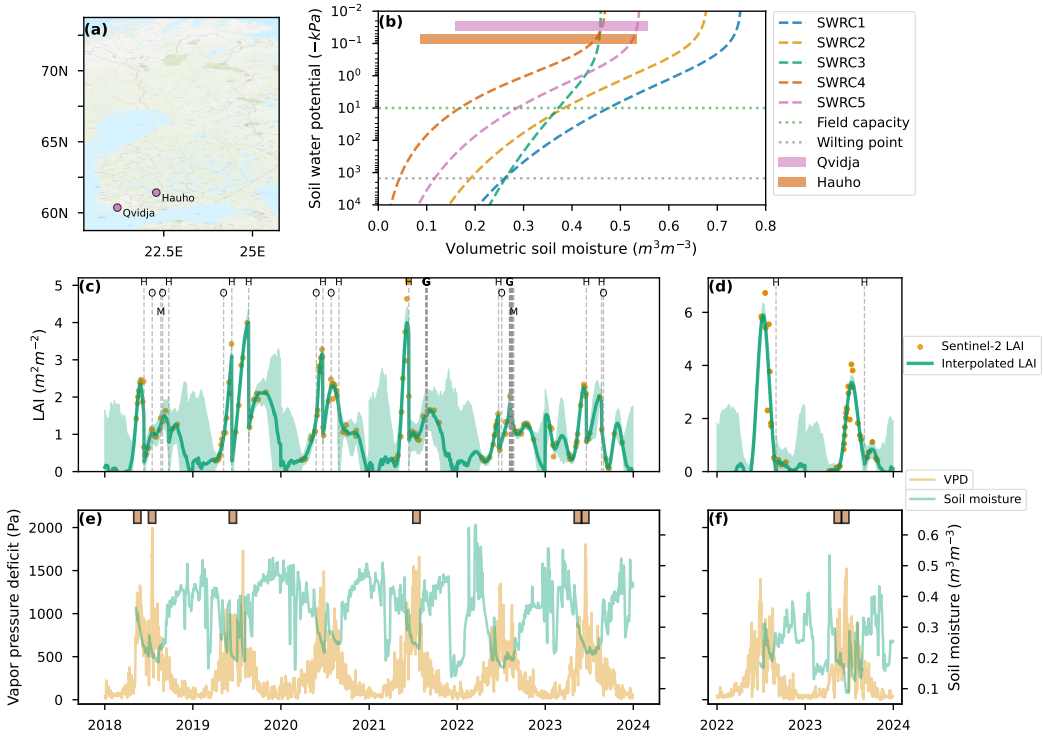

Figure 2. The location of the study sites (a), the five representative soil water retention curves (dashed lines) found for Finnish forest soils (Launiainen et al., 2022) together with the measured range of volumetric soil moisture (colour bars) at the study sites (b), the observed leaf area index (LAI) from Sentinel-2 (dots) and daily LAI (line) interpolated for Qvidja (the GRASS site) (c) and Hauho (the OAT site) (d) using Gaussian-process-regression interpolation (Vira et al., 2025), and the daily vapor pressure deficit and soil moisture observed at the GRASS and OAT sites are shown in (e) and (f). The management events included in the simulations are shown in (c) and (d). H: Harvest; O: Organic fertilizer; G: Grazing. The drought events recognised by the Standardised Precipitation-Evapotranspiration Index (SPEI) (<-1.5) from global SPEI database (https://spei.csic.es/database.html) are also denoted by brown bars in (e) and (f).

water storage (Methods S3) and reproduce observed surface soil moisture dynamics at both sites (Fig. S1). Parameters for the soil water retention function (Eq. 13) were selected by comparing observed volumetric soil moisture range measured with soil water retention curves (SWRC) established for the major Finnish soil types by Launiainen et al. (2022) (Fig.2b). It is shown that SWRC5 and SWRC4 best encompass the observed range of soil moisture at Qvidja and Hauho, respectively, and were therefore chosen for the control simulations. The lower wilting point of SWRC4 for the Hauho site is consistent with the coarser soil texture at Hauho. SWRC3 was additionally tested at Qvidja because it produces lower soil water potentials, and thus stronger water stress, at a given volumetric soil moisture that SWRC5 (Fig. 2b), allowing the sensitivity of modelled crop responses to soil water stress to be evaluated at the study site.

The model simulations were set to start on 01.01.2018 for Qvidja and 01.01.2022 for Hauho, respectively. Both simulations ended on 31.12.2023. As the model simulations started in winter, soil moisture was initialized with a full saturation state, which

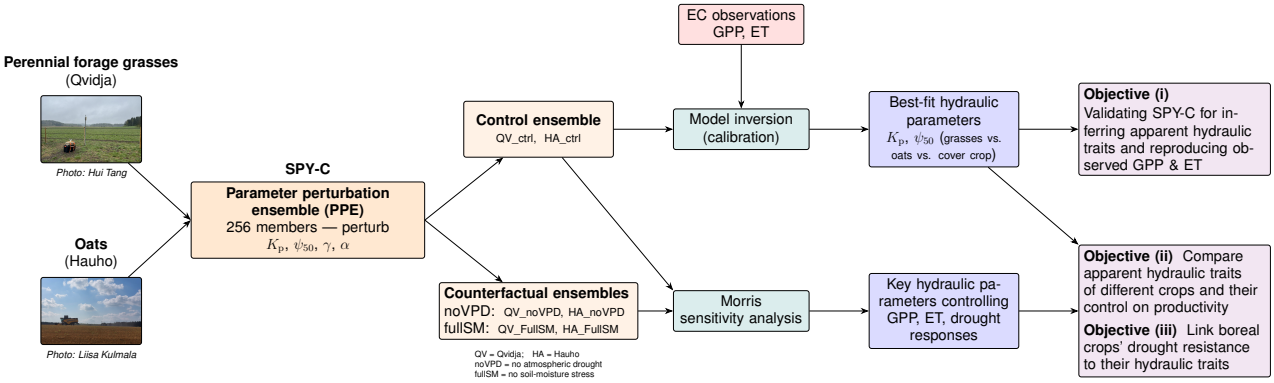

Figure 3. Workflow of using the SPY-C parameter perturbation ensemble (PPE) experiments at two boreal crop sites to address the objectives of this study.

is consistent with soil moisture measurements at the study sites (Fig. 2e,f). The initialization of the soil organic carbon pools in SPY-C was performed by firstly assuming the relative fractions of the four faster-cycling carbon pools in YASSO are in a steady state with a fixed litter carbon composition according to the study by Palosuo et al. (2015) and mean climatology. Meanwhile, the slowest-cycling carbon pool (humus) was set to hold a prescribed carbon fraction (referred to as legacy carbon) that does not equilibrate with the input carbon. Secondly, the relative fractions of different soil carbon pools were rescaled to match the observed total soil organic carbon stock in the 0-100 cm soil layer, which was set to 16.0 (measured range: 14.3–18.8) kg m^{-2} for the Qvidja site (Heimsch et al., 2021), and 12.0 (measured range: 8.5–15) kg m^{-2} for the Hauho site (Fig. S2). We tuned the legacy carbon fraction to match the observed $RECO$ flux at both Qvidja and Hauho, and the values were 0.3 and 0.1 for the Qvidja and Hauho sites, respectively. The lower fraction of the legacy carbon (i.e., the most recalcitrant carbon pool) for the Hauho site is in line with its coarser soil texture and thus less mineral-protected stable carbon (Haddix et al., 2020).

2.2.3 Parameter perturbation ensemble and sensitivity analysis

Although the studied fields (i.e., EC flux footprints) contained mixtures of crop species, these species were spatially well mixed and were therefore represented in the model as a single effectively homogeneous canopy. This treatment is consistent with the model's field-scale representation and allows the inference of apparent hydraulic traits, whereby one effective trait set is estimated for each footprint and study period. To infer these traits and assess their impacts on productivity and drought resistance at each field, we selected four tunable Phydro parameters for parameter perturbation ensemble (PPE) experiments (Table 2). Three parameters, K_p, ψ_{50}, and γ, characterize plant hydraulic properties or strategies, whereas α represents the photosynthetic cost associated with maintaining photosynthetic capacity.

For each PPE, four evenly spaced values were drawn from the prior range of each parameter and combined factorially, yielding 256 ensemble members. The prior ranges of each parameter were defined based on the literature. For the conceptual P-hydro parameters α and γ, the ranges were directly from Joshi et al. (2022), who examined a broad set of plant species: [0.03,

0.12] for α and [0.1,5] (μ mol $m^{-2}s^{-1}Pa^{-2}$) for γ. For the hydraulic parameters K_p and ψ_{50}, Joshi et al. (2022) reported ranges of $[0.2, 15.9]e^{-16}$ m and $[-2.2, -0.4]$ MPa, respectively. Because relatively few herbaceous species were included in that study, we refined these priors using observational studies of herbaceous crops (Table S3). Accordingly, K_p was set to [0.5, 10]e^{-16} m and ψ_{50} to $[-3, -1]$ MPa. These ranges encompass values reported for crops while remaining sufficiently broad to avoid overly constraining the parameter space.

The main PPE experiments performed in this study are summarised in Table 1. For the Qvidja site, two PPE experiments were performed: One using SWRC5 (QV_ctrl) and one using SWRC3 (QV_swrc3). To further separate the impact of soil drought from that of atmospheric drought, two additional sets of PPE experiments were performed: One using fully saturated soil moisture (QV_fullSM) and one using very low VPD (<=50 Pa) (QV_noVPD) for the whole simulation periods. The impact of soil (atmospheric) drought can then be deduced by the difference between QV_fullSM (QV_noVPD) and QV_ctrl. The PPE experiments performed for the Hauho site (HA_ctrl, HA_fullSM, HA_noVPD) were the same as those for the Qvidja site, except that SWRC4 was used in all its PPEs (Table 1).

Table 1. Summary of the settings of the major parameter perturbation ensemble (PPE) experiments performed and analyzed in this study.

Experiments ID	Sites	Crop types	Phydro Parameters	SWRC	Soil moisture	VPD
QV_ctrl	Qvidja	Perennial grass mixture	PPE(256)	SWRC5	Prognostic	Observed
QV_swrc3	Qvidja	Perennial grass mixture	PPE(256)	SWRC3	Prognostic	Observed
HA_ctrl	Hauho	Oats and cover crop	PPE(256)	SWRC4	Prognostic	Observed
QV_fullSM	Qvidja	Perennial grass mixture	PPE(256)	SWRC5	Saturated	Observed
HA_fullSM	Hauho	Oats and cover crop	PPE(256)	SWRC4	Saturated	Observed
QV_noVPD	Qvidja	Perennial grass mixture	PPE(256)	SWRC5	Prognostic	<=50 Pa
HA_noVPD	Hauho	Oats and cover crop	PPE(256)	SWRC4	Prognostic	<=50 Pa

The PPE experiments QV_ctrl and HA_ctrl were used for model inversion to infer the apparent hydraulic traits of the crops at each study site by indentifying the ensemble members that best reproduced the observed daily GPP and ET fluxes (Fig. 3). Because plant photosynthesis and hydraulics are tightly coupled, we employed both GPP and ET fluxes to provide stronger constraints on the four perturbed P-hydro parameters than would be possible using either flux alone. Model performance for each PPE member was evaluated using the Pearson correlation coefficient (cor) and normalized mean square error ($NMSE$) (Eqs. 24 and 25. The five members that ranked highest in cor and lowest in $NMSE$ jointly for GPP and ET were selected, and their corresponding Phydro parameter sets were interpreted as the best-fit apparent hydraulic traits of each crop. Details of the ranking procedure are provided in Methods S4. Both cor and $NMSE$ were calculated from daily data to emphasize the model's ability to reproduce daily variabilities and subseasonal drought responses. Using monthly data yielded similar

parameter rankings and is therefore not shown here.

$$cor = \frac{\sum_{i=1}^{n}(X_{obs,i} - \mu_{obs})(X_{sim,i} - \mu_{sim})}{\sqrt{\sum_{i=1}^{n}(X_{obs,i} - \mu_{obs})^2 \sum_{i=1}^{n}(X_{sim,i} - \mu_{sim})^2}} \tag{24}$$

$$NMSE = \frac{\sum_{i=1}^{n}(X_{obs,i} - X_{sim,i})^2}{\sum_{i=1}^{n} X_{obs,i}^2}, \tag{25}$$

where i is the time step and n is the total number of time steps, $X_{obs,i}$ and $X_{sim,i}$ are the observed and simulated values at each time step, μ_{obs} and μ_{sim} are the respective mean values over all time steps. Here, the time periods used to calculate these matrices correspond to the model inversion periods for inferring apparent hydraulic traits and were therefore selected separately for each crop. Specifically, the inversion periods were 01.2019–12.2022 for the forage grass mixture at Qvidja and 06.2022–12.2023 for oats at Hauho. For the cover crop at Hauho, the inversion period was 09–10.2023, when it was actively growing and had become dominant in the field. At Qvidja, year 2018 and 2023 were excluded from the inversion period because sowing events in those years may have altered species composition. Instead, these years were used as independent tests of whether the inferred apparent hydraulic traits were transferable beyond the inversion periods. Additional analyses using alternative inversion periods are described in Methods S4.

To detect the effects of crop hydraulic traits on crop performance and drought response, the Morris sensitivity analysis (Morris, 1991) was also conducted using the PPE experiments for both sites, including both the control and counterfactual PPEs (Fig. 3). The sensitivities of monthly GPP, ET, and water use efficiency (WUE) to the 4 Phydro parameters perturbed in PPE were quantified. Here, WUE was measured at both the plant level ($pWUE$, unit: $\mu\mathrm{mol\ CO_2\ (mmol\ H_2O)^{-1}}$) as given by:

$$pWUE = GPP/Tr, \tag{26}$$

and the leaf level, often called intrinsic WUE ($iWUE$, unit: $\mu\mathrm{mol\ CO_2\ (mmol\ H_2O)^{-1}}$) as given by:

$$iWUE = (A_j + R_d)/1.6g_s. \tag{27}$$

The Morris method is an efficient global sensitivity analysis technique for parameter screening (Campolongo et al., 2007), especially with a limited sampling size (Gan et al., 2014). It is similar to the commonly used one-at-a-time sensitivity analysis, yet also considers the interactions among parameters. The overall effect and interaction effect of each parameter are approximated by the mean (mu) and standard deviation ($sigma$) of the elementary effects of each parameter sampled. In addition, the mean of absolute effects (mu^*) is also used to indicate if the elementary effects are of opposite signs (Campolongo et al., 2007). The analysis was performed using the Python package SALIB, version 1.4.8 (Herman and Usher, 2017).

Table 2. Summary of the prior ranges of the Phydro parameters used in parameter perturbation ensemble (PPE) experiments. The parameter sets corresponding to the five best-fit PPE members for the forage grass mixture at Qvidja (based on QV_ctrl) and for oats and cover crop at Hauho (based on HA_ctrl) are also listed. These parameter sets reflect the effective field-level hydraulic traits (i.e., apparent hydraulic traits) for the dominant crop community within each EC footprint and model-inversion period. K_p: the maximum whole-plant conductance per unit leaf area ($10^{-16}m$). ψ_{50}: the water potential at which 50% of plant hydraulic conductivity (MPa) is lost. α: the unit cost of maintaining photosynthetic capacity. γ: the unit cost of maintaining plant hydraulic pathways. cor_{gpp} and cor_{et}: the correlation coefficients between model and observation for GPP and ET, respectively. $nmse_{gpp}$ and $nmse_{et}$: the normalized mean squre error between model and observation for GPP and ET, respectively.

Parameters	K_p	Φ_{50}	α	γ	cor_{gpp}	$nmse_{gpp}$	cor_{et}	$nmse_{et}$
Prior range	$[0.5, 10]$	$[-3, -1]$	$[0.03, 0.12]$	$[0.1, 5]$				
Five best-fit PPE members								
Perennial grass mixture (Qvidja)	0.5	-1	0.06	3.36	0.940	0.067	0.938	0.158
	0.5	-1.7	0.06	3.36	0.941	0.066	0.939	0.165
	0.5	-1.7	0.03	5.00	0.939	0.081	0.939	0.165
	0.5	-2.3	0.06	5.00	0.941	0.068	0.934	0.142
	0.5	-3.0	0.06	5.00	0.941	0.067	0.935	0.142
Oats (cash crop, Hauho)	0.5	-1.0	0.03	3.36	0.963	0.059	0.905	0.115
	0.5	-1.7	0.03	3.36	0.964	0.056	0.906	0.115
	0.5	-1.7	0.06	1.73	0.965	0.087	0.908	0.123
	0.5	-2.3	0.03	3.36	0.965	0.055	0.907	0.115
	0.5	-3.0	0.03	5.00	0.964	0.059	0.902	0.115
Italian ryegrass (cover crop, Hauho)	3.7	-1.7	0.03	3.36	0.817	0.201	0.785	1.700
	3.7	-3.0	0.06	1.73	0.818	0.245	0.786	1.995
	3.7	-1.0	0.06	1.73	0.812	0.257	0.786	2.065
	6.8	-1.7	0.06	5.00	0.816	0.247	0.787	2.195
	6.8	-1.0	0.06	5.00	0.830	0.250	0.787	2.232

3 Results

3.1 Apparent hydraulic traits at Qvidja and Hauho

We identified five Phydro parameter sets that best reproduced daily GPP and ET at both sites. The results are shown in Table 2. For the perennial grass mixture at Qvidja and oats at Hauho, these best-fit parameter sets, interpreted as apparent field-scale hydraulic traits, were consistently characterized by low K_p but high γ, indicating relatively low hydraulic efficiency and a conservative water-use strategy. A low α (i.e., cost to maintain photosynthetic capacity) was also required to reproduce the observed fluxes for both crops, implying relatively high photosynthetic capacity (Fig. S3). Compared with the perennial grass, oats showed slightly lower best-fit α and γ values (Table 2), pointing to higher photosynthetic capacity and a more acquisitive

hydraulic strategy. The cover crop at Hauho exhibited higher inferred K_p, indicating greater hydraulic efficiency than either oats or the perennial grass mixture. In contrast, no clear preference for ψ_{50}, a commonly used indicator of hydraulic safety, emerged across the studied crops, whereas the other three Phydro parameters were more strongly constrained.

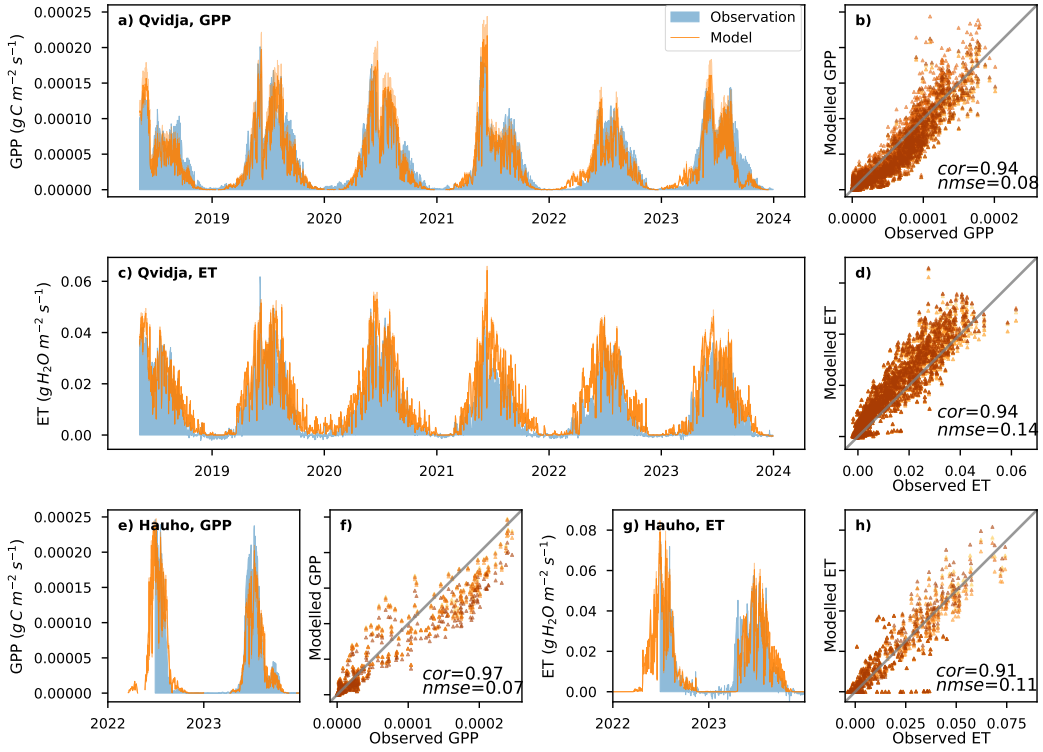

Figure 4. (a-d) Daily mean gross primary production (GPP) and evapotranspiration (ET) modelled by the five best-fit PPE members from QV_ctrl and HA_ctrl (see Table 2) and their comparison with observation at the Qvidja (a-d) and Hauho (e-h) site, respectively. The modelling results based on the five best-fit PPE members of QV_swrc3 can be found in Fig. S4.

Fig. 4e–l show how the five best-fit PPE members selected for the perennial grass mixture and oats perform in simulating daily GPP and ET at the study sites. Overall, the simulated GPP and ET matched the observed fluxes very well, with $cor \approx 0.94$ and $NMSE \leq 0.14$ for the Qvidja site, and $cor \geq 0.91$, $NMSE \leq 0.11$ for the Hauho site. Only a slight overestimation of daily ET was observed at the Qvidja site (Fig. 4h), and a mismatch of ET occurred at the OAT site in the early spring 2023 when the model failed to capture the observed high ET (Fig. 4k), largely due to the bias in the onset of snowmelt in the meteorological forcing data (Fig. S7). The observed diurnal cyles of GPP and ET in summer were also well captured by the best-fit PPE members (Fig. 5), except that there was a slight underestimation (overestimation) of GPP (ET) in early morning and late afternoon, probably resulting from a different light absorption rate from what was assumed in the model (see Eq. 8) due to the low sun angle.

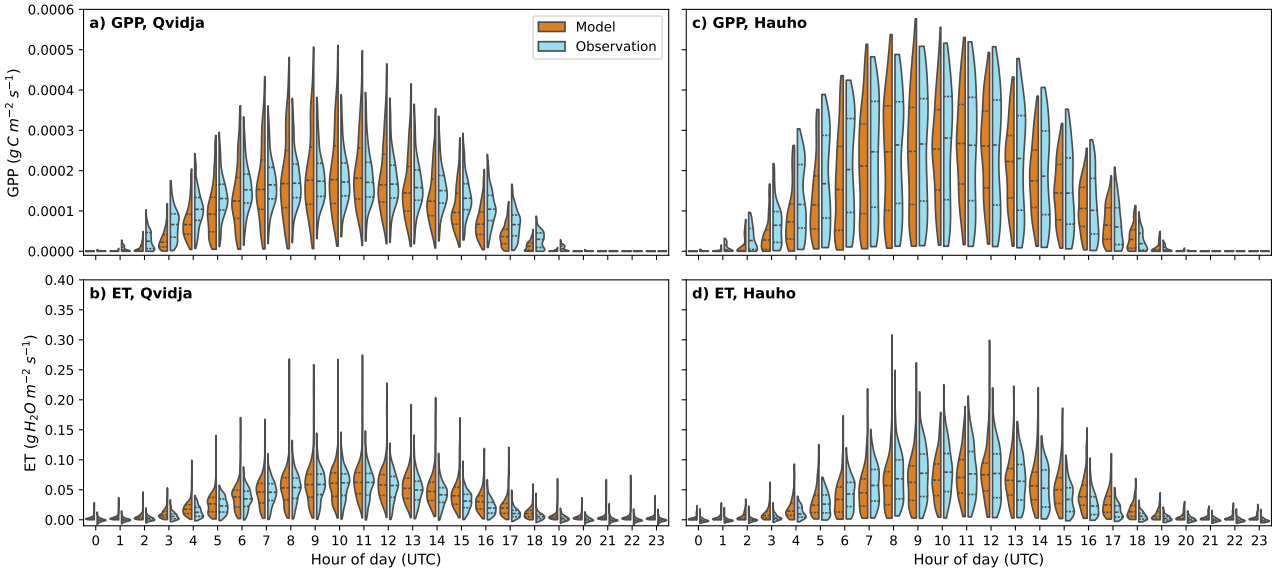

Figure 5. Daily cycle of gross primary productivity (GPP) and evapotranspiration (ET) fluxes in summer (June, July and August) modelled by the average of the five best-fit PPE members from QV_ctrl and HA_ctrl and their comparison with observation at Qvidja (a,b) and Hauho (c,d), respectively. The violin denotes the distribution of the hourly values in all the summer days and the horizontal lines in the violins denotes the 25th, 50th (median), and 75th percentiles.

We further examined the results of the five best-fit PPE members in the context of the full PPE experiments spanning a wide hydraulic and photosynthetic trait space (Fig. 6). For GPP, the best-fit PPE members generally fell in the upper range of the full PPE (Fig. 6a, b), except in May at the Qvidja site when they shifted towards the lower end of the spread. But for ET, the best-fit PPE members tended to lie in the lower range (Fig. 6c, d), except during dry summer months, such as June 2018, 2019, 2023, July 2021 at Qvidja and July–August 2022 at Hauho. Consequently, their monthly mean pWUE and iWUE were close to the upper limit of the PPE, except in those same drought periods (Fig. 6e–h). Notably, the soil moisture simulated in the best-fit PPE members consistently lies in the upper range of the PPE (Fig. 6i–j), far above the wilting point.

3.2 Sensitivity of crop performance to hydraulic traits

The Morris sensitivity analysis of GPP, ET, pWUE, and iWUE to the four Phydro parameters in QV_ctrl and HA_ctrl is shown in Fig. 7a–h. The sensitivities are context-dependent and vary seasonally, but do not differ much between the two study sites. GPP is dominated by negative sensitivity to α (the cost to maintain photosynthetic capacity) throughout the growing season, except in June–July, when K_p and γ exert strong negative and positive effects, respectively, suggesting that lower hydraulic efficiency can promote crop productivity during these months. ET, pWUE, and iWUE exhibit more pronounced sensitivity to the hydraulic parameters (i.e., K_p and γ). In particular, K_p (γ) can negatively (positively) influence pWUE and iWUE in May,

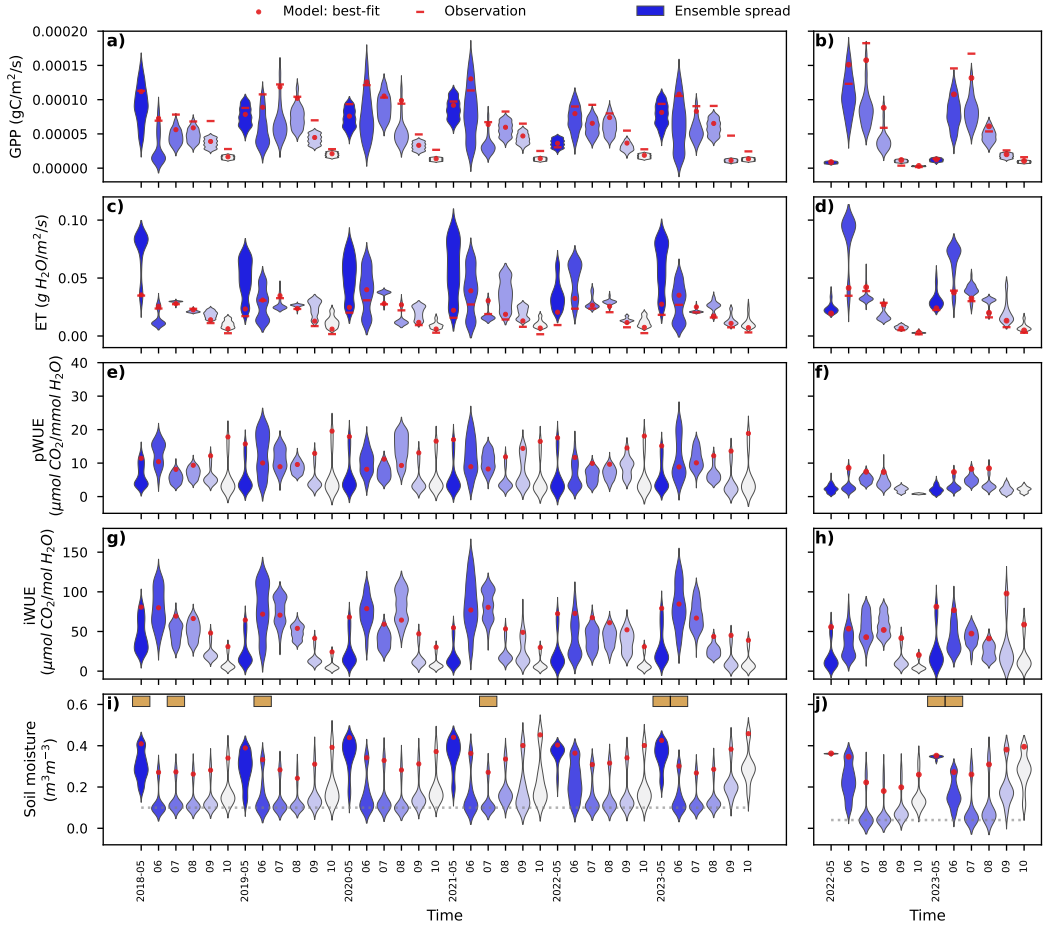

Figure 6. The violin plots showing the spread of monthly mean gross primary production (GPP), evapotranspiration (ET), water use efficiency (pWUE and iWUE), and bulk root-zone soil moisture in the PPE for Qvidja (QV_ctrl) (a, c, e, g, i) and Hauho (HA_ctrl) (b, d, f, h, j). The width of the violin denotes the probability density of the ensemble members that yield the same values. The red circles represent the mean of the five best-fit PPE members. The red bars in (a-d) denote the observation. The brown boxes in (i) and (j) denote drought events according to Standardised Precipitation-Evapotranspiration Index (SPEI) less than -1.5. The dotted line in (i) and (j) denote the wilting point (i.e., the soil moisture at -1.5 MPa matric potential). The results from another PPE of Qvidja, i.e., QV_swrc3 can be found in Fig. S5.

September, and October, while the effects often reverse in summer, highlighting a positive impact of hydraulic efficiency on pWUE and iWUE at peak growth, which is opposite to its impact on GPP.

We note that while the effects of α are quite independent of the other parameters (low $Sigma$), the effects of K_p and γ are more dependent on the other parameters (high $Sigma$), indicating strong coordination among crop hydraulic traits. We observe little influence of ψ_{50} on GPP, ET, and WUE at both study sites, but a noticeable positive effect on soil moisture in summer (Fig.

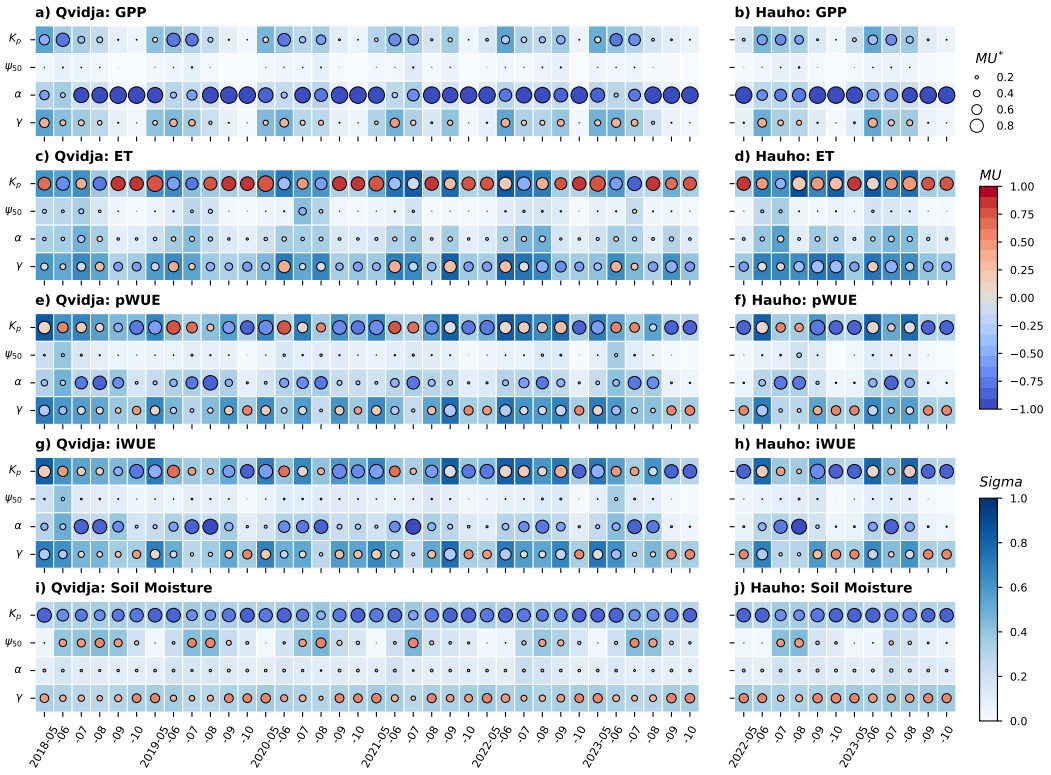

Figure 7. Morris' sensitivity analysis of monthly averaged gross primary production (GPP) (a, b), evapotranspiration (ET) (c, d), plant-level water use efficiency (pWUE) (e, f), internal water use efficiency (iWUE) (g, h) and bulk root-zone soil moisture (i, j) to Phydro parameters (K_p, ψ_{50}, α, and γ) in the PPE for Qvidja (QV_ctrl) and Hauho (HA_ctrl) during growing season (May-October). The mean of the absolute elementary effect (MU^*) is denoted by the sized of the circle. The mean of the elementary effect (MU) is denoted by the colour shading of the circle. The standard deviation of the elementary effect ($Sigma$) is denoted by the colour shading of the rectangles. The results of QV_swrc3 can be found in Fig. S6 in the SI.

7i, j). A uniform negative (positive) effect of K_p (γ) on soil moisture (Fig. 7i, j) suggests that lower crop hydraulic efficiency can better conserve soil water from being withdrawn by the crop.

3.3 Response to soil and atmospheric drought

As illustrated in Fig. 8, the removal of soil drought and VPD increases GPP during the summer months in most members of PPE (Figs. 8a–d) with the magnitude of the increase positively related to K_p. In contrast, transpiration responds differently to the absence of soil versus atmospheric droughts (Fig. 8e–h): removing soil drought produces a consistently positive change, whereas reducing atmospheric drought induces a large spread with both positive and negative responses. Changes in transpiration are again most sensitive to K_p with positive effects mainly in summer.

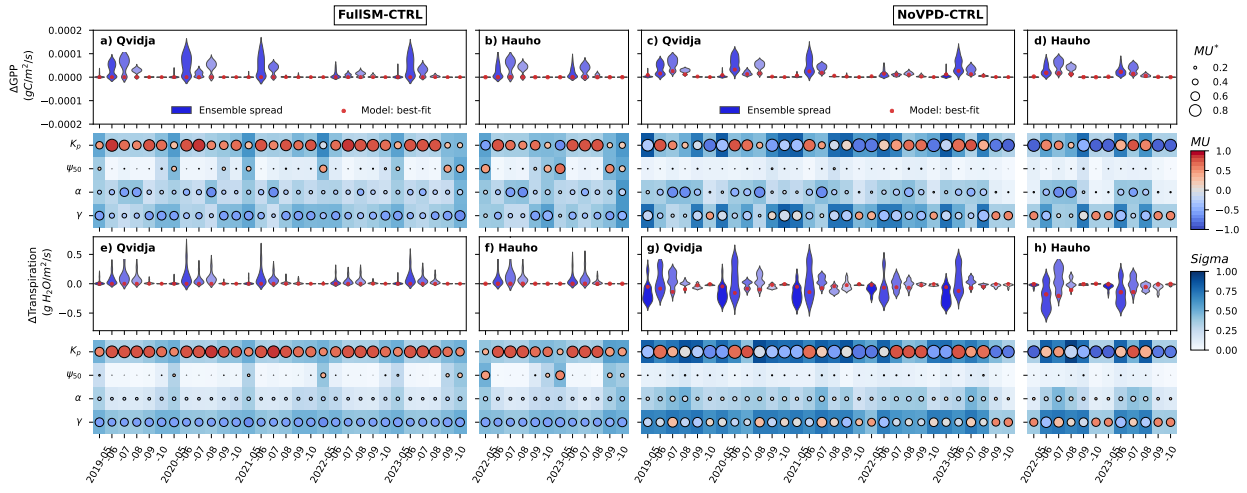

Figure 8. Modelled response of monthly averaged gross primary production (GPP) and transpiration to the removal of soil drought (FullSM-CTRL) (a, b, e, f) and the removal of atmospheric drought (NoVPD-CTRL) (c, d, g, h) at both Qvidja (a, c, e, g) and Hauho (b, d, f, h). **FullSM**: QV_fullSM and HA_fullSM; **NoVPD**: QV_noVPD and HA_noVPD; **CTRL**: QV_ctrl and HA_ctrl. The upper panel of each subplot shows the spread of the ensemble experiments (violins), and the mean of the five best-fit PPE members (red dots). The lower panel of each subplot shows the Morris sensitivity of the simulated responses to the Phydro parameters (K_p, ψ_{50}, α, and γ).

The five best-fit PPE members display little change in GPP and transpiration when soil drought is removed (Figs. 8a, b, e, f), indicating that crop photosynthesis and transpiration may have not suffered from soil drought, even though drought events were widely observed at the study sites (Fig. 6i, j). In contrast, a discernible rise in GPP and a reduction in transpiration during summer is shown in these best-fit PPE members when atmospheric drought is removed (Figs. 8c, d, g, h), suggesting that VPD may have exerted a more prevalent effect on crop performance than soil drought at the study sites.

The effect of VPD is further manifested in Fig. 9, where the five best-fit PPE members from QV_ctrl, HA_ctrl and QV_swrc3 dispay a clear impact of VPD on photosynthetic assimilation rate, pWUE, and iWUE (Fig. 9b, o, p) at daily time scale. This can be associated with its strong regulation of stomatal conductance (Fig. 9d) and particularly soil-leaf water potential difference (Fig. 9l), which further impact leaf internal-to-external CO_2 ratio (χ) (Fig. 9h) and thus carboxylation and electron-transport capacity (Fig. 9f, j). The modelled effect of VPD appears to be quite non-linear: while the impact on hydraulic behaviours, such as stomatal conductance, pWUE, and iWUE, mainly occurs in the early phase of VPD increase (VPD$\leq$0.8 kPa) (Fig. 9d, h, i, n, p), the downregulation of photosynthetic activity emerges only in the later phase (VPD$\geq$0.8 kPa) (Fig. 9b, f, j).

In comparison, soil drought and its impacts are hardly shown in the five best-fit PPE members, as soil water potential in these simulations remains well above the wilting point (Fig. 9a, c), except those from QV_swrc3 with. a more drought-prone SWRC. When soil moisture approches the wilting point, photosynthetic capacity, assimilation rate, and stomatal conductance (Fig. 9a, c, e, i) decrease drastically, but pWUE and iWUE increase with lower soil water potential (Fig. 9m, o). Such response contrasts with the effect of increasing VPD, which tends to promote iWUE but reduce pWUE (cf. Fig. 9m, o and n, p).

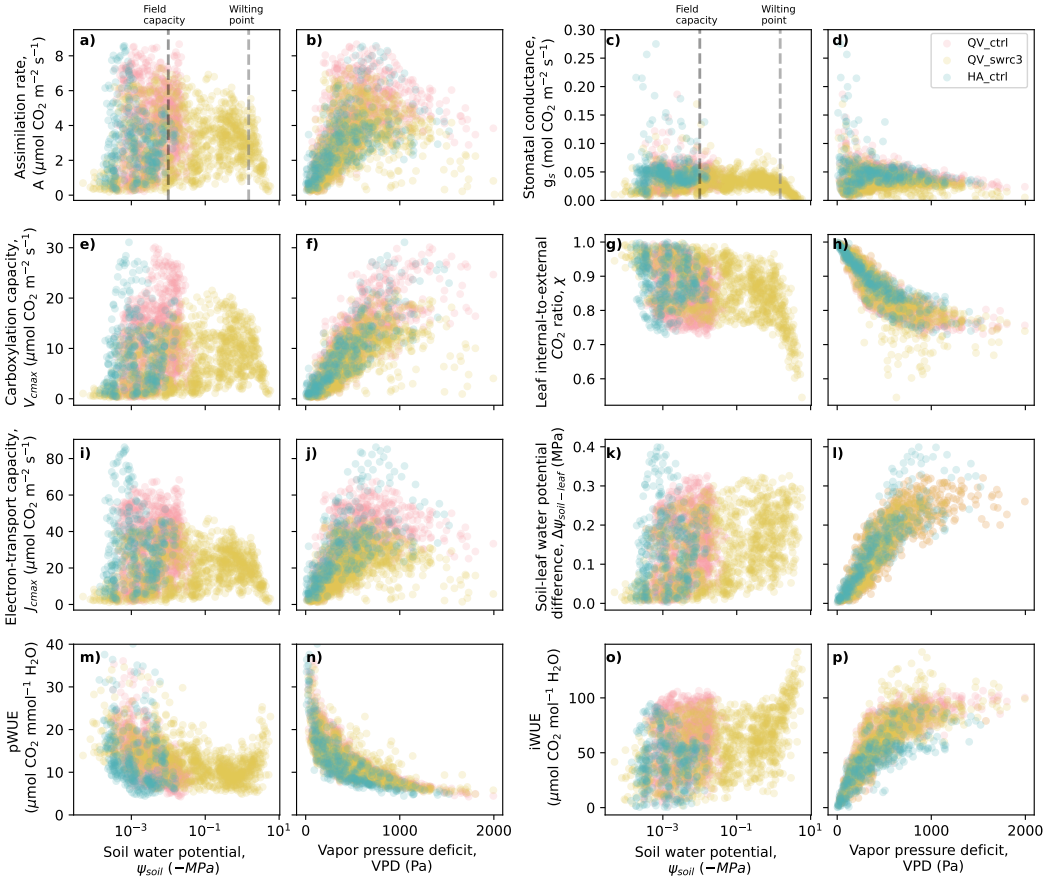

Figure 9. Daily response of photosynthetic and hydraulic variables to soil water potential (first and third column) and vapor pressure deficit (second and fourth column) simulated in the five best-fit PPE members selected from QV_ctrl, QV_swrc3, and HA_ctrl. (a,b) assimilation rate (A, μmol CO_2 m^{-2} s^{-1}), (c,d) stomatal conductance (g_s, mol CO_2 m^{-2} s^{-1}), (e,f) leaf internal-to-external CO_2 ratio (χ), (g,h) soil-leaf water potential difference ($\Delta\psi_{soil-leaf}$, MPa), (i,j) Carboxylation capacity (V_{cmax}, μmol CO_2 m^{-2} s^{-1}), (k,i) Electron-transport capacity (J_{max}, μmol CO_2 m^{-2} s^{-1}), (m,n) plant-level water use efficiency (pWUE, μmol CO_2 $(\text{mmol } H_2O)^{-1}$), (o,p) intrinsic water use efficiency (iWUE, μmol CO_2 $(\text{mol } H_2O)^{-1}$).

4 Discussion

4.1 Apparent hydraulic traits of boreal crops

Crop hydraulic traits have often been overlooked in boreal crop studies (Roitsch et al., 2022). By employing SPY-C and EC flux measurements, we were able to infer apparent hydraulic traits at the field scale and assess their impacts on crop performance under typical boreal conditions. Constrained by both observed carbon and water fluxes, the maximum hydraulic conductance (K_p) inferred for both the perennial forage grass mixture and the annual cereal (oats) was toward the lower end of values

reported for crop species (cf., Table 2 and Table S3), suggesting relatively low hydraulic efficiency and a conservative water-use strategy. This contrasts with the relatively high hydraulic efficiency reported for many crops (Table S3), but is consistent with the lower hydraulic efficiency documented in boreal plant species. This similarity implies that adaptation to boreal climatic conditions may have favour conservative water-use strategy in boreal crops.

Consistent with the low hydraulic conductance, the hydraulic safety margin, defined as the difference between the minimum leaf water potential experienced during the growing season (ψ_{min}) and ψ_{50} (Choat et al., 2012; Anderegg et al., 2018), remained well above zero despite the large uncertainties in ψ_{50} (Fig. S9). This points to a high resistance of the studied crops to the drought present in current climate conditions. We also found relatively low stomatal conductance (Fig. 9) and a faster decline in leaf water potential than in soil water potential, an indicator of anisohydric stomatal behaviour (Fig. S8a). Stomatal closure generally occurs after significant loss of hydraulic conductivity (Fig. S9), implying a relatively "risky" stomatal regulation and a low stomatal safety margin (Gleason et al., 2022; Martin-StPaul et al., 2017; Pereira et al., 2024). These model-inferred behaviours are broadly concur with empirical evidence from perennial forage grasses (e.g. Holloway-Phillips and Brodribb, 2011b; Jacob et al., 2022) and some cereal crops (e.g. Corso et al., 2020).

The inferred apparent hydraulic traits of both crops show little variation when using different model-inversion periods (Fig. 4 and Methods S4), consistent with evidence that hydraulic traits can be relatively conserved features within species (Lamy et al., 2014). We also inferred a slightly more acquisitive water-use strategy (e.g., lower γ and higher K_p) for the annual cereal crop (oats) and the cover crop dominated by annual ryegrass than for the perennial forage grass mixture (timothy, meadow fescue, and white clover) (Table 2 and Fig. 4a–d), in broad agreement with the empirical evidence summarized in Table S3.

To further evaluate the plausibility of the inferred apparent hydraulic traits, we acompared the modelled responses of stomatal conductance and whole plant water conductance to changes in leaf water potential with available empirical observations. As shown in Fig. 10, the model inferred lower maximum hydraulic conductance (K_p) and stomatal conductance for perennial forage grass than reported (Fig. 10a,d). Agreement improved at lower leaf water potentials. One possible reason for such discrepancy can be the difference in scale: model-inferred K_p reflects the whole-plant hydraulic conductance at field level, whereas empirical studies typically measure leaf-level conductance of individual plant. Differences in species, cultivars, and climatic origin may also contribute, as the available measurements were all from temprate rather than boreal cultivars. Additional hydraulic measurements of Nordic crops are therefore needed to better constrain and evaluate the modelled-inferred hydraulic traits and behaviours.

For oats and Italian ryegrass, the model generally captured the observed stomatal responses to declining leaf water potential (Fig. 10b, c), except that the observation exhibited more rapid stomatal closure during dehydration than predicted by the model for Italian ryegrass, indicating more isohydric behaviour. A higher ψ_{50} (i.e., -1 MPa) produced a closer match to the observed response to leaf dehydration. As values above -1 MPa have recently been reported for some crops (Cardoso et al., 2025), increasing ψ_{50} above -1 MPa may further improve the model results. Increasing γ, the cost of maintaining hydraulic pathways, also shifted the simulated response toward more isohydric behaviour (data not shown). These sensitivities highlight the need for direct hydraulic measurements of boreal crops to better constrain both ψ_{50} and γ and to assess the remaining model–observation discrepancies.

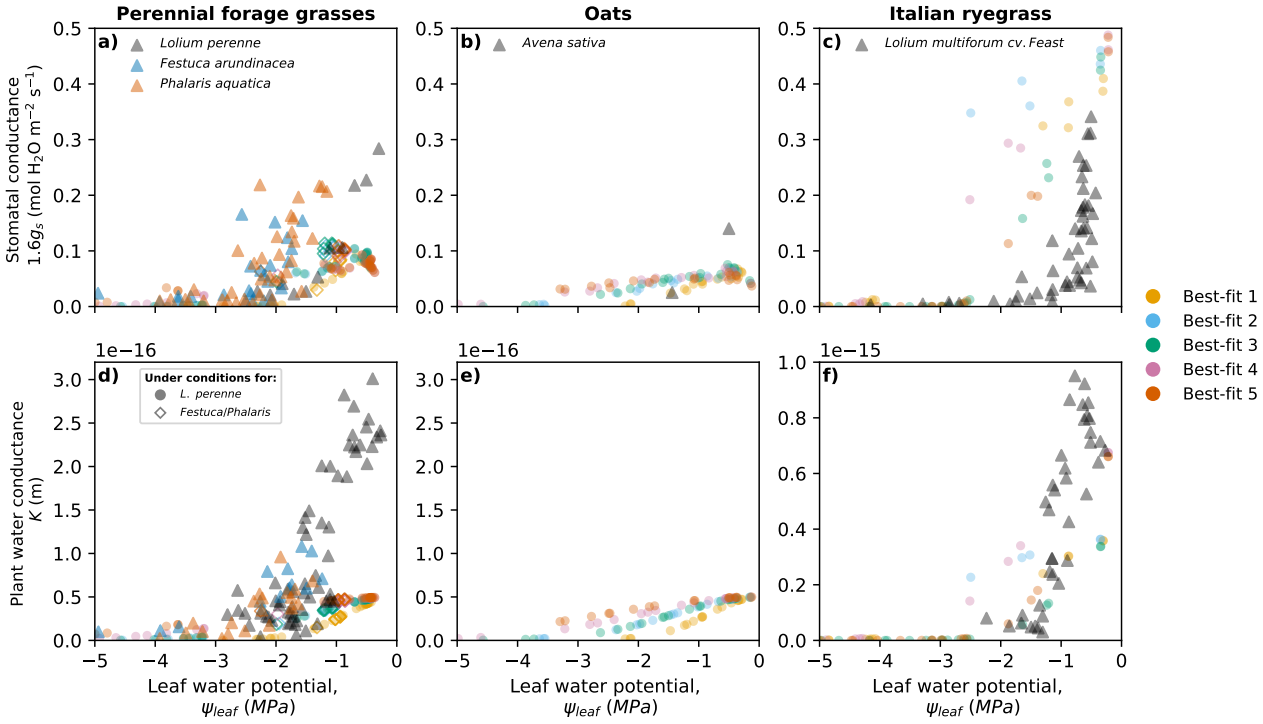

Figure 10. The modelled response of stomatal conductance ($1.6 \times g_s$, μmol H_2O m^{-2} s^{-1}) (a-c) and plant water conductance (K, $10^{-16} m$) (d-f) to the decline of leaf water potential (ψ_{plant}, MPa) and their comparison with observation of similar crops from literature. (a,d) are for forage grasses, (b,e) are for oats and (c,f) are for cover crop. The modelled results (small circles) correspond to the QV_swrc3 PPE members using the five best-fit parameter sets listed in Table 2 for each crop, with best-fit members 1–5 following the same order as in the table. We use the QV_swrc3 PPE here because it produces a wider range of leaf water potential, allowing hydraulic responses to be more clearly evaluated. The empirical data are denoted by triangles, which are from Holloway-Phillips and Brodribb (2011b) (*Lolium perenne*), Jacob et al. (2022) (*Festuca arundinacea*, *Phalaris aquatica*), Canales et al. (2021) (*Avena sativa*) and Holloway-Phillips and Brodribb (2011a) (*Lolium multiforum cv. Feast*). The hourly model data within the growing season (May–October, 2018–2023) that matched the environmental conditions of the corresponding leaf gas-exchange measurements were selected. *L. perenne* and *L. multiflorum*: VPD 1.35–1.65 kPa, PAR 900–1100 μmol m^{-2} s^{-1}, and temperature 18–22 °C; *F. arundinacea* and *P. aquatica*: VPD 1–2 kPa, PAR 1620–1980 μmol m^{-2} s^{-1}, and temperature 26–30 °C; *A. sativa*: VPD 0.72–0.88 kPa, PAR 225–275 μmol m^{-2} s^{-1}, and temperature 18–22 °C.

4.2 Role of hydraulic coordination in crop productivity and drought resistance

The low hydraulic efficiency was found to be critical for achieving a high GPP in summer when both soil and atmospheric drought were present, co-limiting crop productivity (Fig. 6). Under such conditions, crops with low hydraulic efficiency deplete soil moisture more slowly, thereby preventing soil moisture from being depleted to its critical threshold that significantly limits productivity (Fig. 6i, j and Fig. 7i, j). This advantage largely disappeared when either soil or atmospheric drought was removed (Fig. S10 and S11), indicating that the effect of hydraulic efficiency on productivity is strongly environment dependent.During

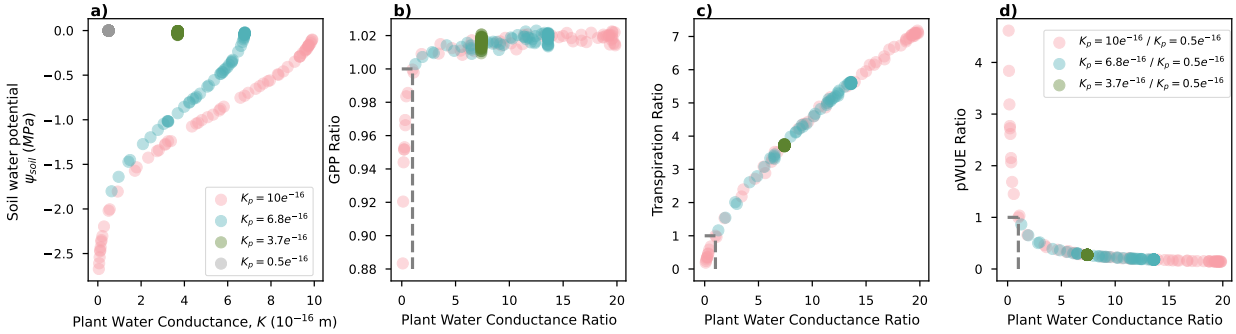

Figure 11. The relation between plant water conductance (K, $10^{-16}m$) and soil water potential (ψ_{soil}, MPa) (a), the ratio of plant water conductance and the ratio of GPP (b), transpiration (c), and pWUE (d). The ratios were calculated between simulations with higher K_p and that with lowest K_p ($0.5e^{-16}$). They are all from the PPE of QV_noVPD (). The intersection of the horizontal and verticle grey dashlines in (b, c, d) denotes the reference point where the ratio equals to 1.

the cool and wet months, e.g. May, higher hydraulic efficiency tend to promote GPP (Fig. 7a, b), consistent with previous studies reporting positive relationships between hydraulic efficiency and productivity (Holloway-Phillips and Brodribb, 2011a; Ocheltree et al., 2016; Gleason et al., 2021). However, under drought conditions in summer, our results agree with the studies showing that conservative water use (i.e., lower hydraulic efficiency) can sustain higher crop yields by avoiding excessive water depletion (Holloway-Phillips and Brodribb, 2011a; Gleason et al., 2022; Schell et al., 2025).

The effect of hydraulic efficiency (K_p) on plant water-use efficiency (pWUE) was more complex (cf. Fig. 7a,b and e,f) because carbon uptake and transpiration responded differently to hydraulic limitation (Fig. 11). Accordingly, hydraulic strategies that favoured GPP did not necessarily maximize pWUE (Fig. 6), underscoring the challenge of optimizing both GPP and pWUE in crops under drought conditions (Leakey et al., 2019; Yu et al., 2020). In our simulations, higher hydraulic efficiency tended to increase pWUE during summer water deficit but decrease it during wetter spring and autumn conditions (Fig. 7e, f). This is in agreement with the contrasting effects of hydraulic efficiency reported in a previous study on annual ryegrass (see Table 4 in Holloway-Phillips and Brodribb, 2011a). Under soil drought, high hydraulic efficiency accelerated soil-water depletion and lowered soil and plant water potentials (Fig. 11a). The resulting decline in hydraulic conductance reduced both GPP and transpiration, but transpiration declined more strongly, thereby increasing pWUE (Fig. 11b-d). GPP remained relatively insensitive until soil water potential fell below approximately the wilting pont (-1.5 MPa), after which photosynthesis also declined more markedly.

Overall, our modelling results indicate that atmospheric drought exerted a much stronger effect on crop productivity than soil drought at the two study sites (Fig. 8). Little evidence of soil-water limitation was found in the best-fit members from the PPEs using the baseline soil hydraulic parameterizations (i.e., QV_ctrl and HA_ctrl), whereas substantial soil drought effects emerged only in the best-fit members of the PPE with more drought-prone soil water rentention curve (i.e., QV_swrc3) (Fig. 9). In contrast, the effects of VPD on productivity and WUE are well demonstrated at both study sites (Figs. 8c, d, g, h and

9). We hence argue that the extensive periods of high VPD may have contributed substantially to the yield reductions observed during drought years at Qvidja (Heimsch et al., 2021), consistent with evidence for a dominant role of atmospheric dryness in regulating plant productivity in the boreal regions (Mirabel et al., 2023; Seddon et al., 2016).

The limited role of soil drought was further supported by the absence of a critical soil-moisture threshold in either the flux observations or the best-fit PPE members from QV_ctrl and HA_ctrl (Fig. S8b–d), following the diagnostic proposed by Fu et al. (2024). Such a threshold appeared only in the best-fit members of QV_SWRC3 at a volumetric soil moisture of approximately 0.3, suggesting that the use of SWRC3 likely overestimated soil drought stress at Qvidja. We note that the current version of SPY-C does not account for potential impacts of soil drought on above- and below-ground carbon allocation, which have been widely recognised in previous studies (Qiao et al., 2021; Xia et al., 2017). Whether such responses occurred at our study sites remains to be investigated. Incorporating a dynamic carbon allocation scheme responsive to soil water availability would help address this limitation.

The weak response of productivity to soil drought can therefore be interpreted primarily as drought avoidance rather than tolerance (Haugum et al., 2021; Alves et al., 2024; Pereira et al., 2024; Cardoso et al., 2025). The relatively low hydraulic efficiency inferred for the studied crops limited rapid soil water depletion and also partly buffered them against atmospheric drought, as evidenced by a positive impact of hydraulic conductance on the response of GPP to the absence of VPD in summer (Fig. 8c,d). However, this buffering became insufficient at daily VPD ≥ 0.8 kPa, when hydraulic adjustment could no longer sustain leaf water balance and both stomatal conductance and photosynthesis declined (Fig. 9b, d, f, g). The relatively risky stomatal regulation and low stomatal safety margin inferred for the studied crops showed no clear association with their drought resistance, consistent with recent findings for herbaceous crops (Pereira et al., 2024).

4.3 Model uncertainties and future development

Several structural simplifications in the current version of SPY-C may contribute to uncertainties in the simulated carbon and water fluxes and the inferred apparent hydraulic traits. First, SPY-C adopts a big-leaf canopy representation, in which prescribed total one-sided green LAI is combined with within-canopy light attenuation using Beer's law. The model therefore does not explicitly distinguish sunlit and shaded leaves or resolve multiple canopy layers. This simplification may contribute to biases in the diurnal partitioning of GPP and ET, particularly during the early morning and late afternoon (Fig. 5). A two-leaf or multilayer canopy representation could improve the treatment of within-canopy radiation and associated carbon and water fluxes.

A second important simplification concerns the representation of roots dynamics and its influence on whole-plant hydraulics. In the current framework, K_p represents the maximum whole-plant hydraulic conductance per unit leaf area and therefore integrates the entire soil-to-leaf hydraulic pathway, including roots and the root–soil interface. Root hydraulic traits are thus represented only implicitly rather than as separate root, stem, and leaf conductances. Moreover, water uptake occurs from a fixed effective root zone (0.6 m in this study), while root biomass is tracked as a carbon pool but does not feed back on rooting depth, water uptake, or hydraulic conductance. Dynamic rooting depth, root distribution, hydraulic redistribution, and drought-induced changes in root hydraulic conductivity are therefore not represented. These processes can play an important

role in drought adaptation of cereals and grasses (e.g. Canales et al., 2021). Coupling dynamic root growth to water uptake and hydraulic conductance, together with prognostic leaf growth, is therefore an important direction for future development. Such extensions would also allow drought avoidance mediated through root-zone dynamics to be represented more explicitly.

Uncertainty also arises from model structural biases, parameterization, and model inversion approach. We note indications that canopy and ground evaporation may be overestimated leading to the overestimation of ET (Fig. 4b, d). However, sensitivity experiments with reduced evaporation did not alter the inferred K_p (data not shown), suggesting that this bias has little influence on the inferred apparent hydraulic traits. Although the PPE approach enabled us to constrain apparent hydraulic traits using both carbon and water fluxes, the present ensembles varied only a limited set of plant hydraulic and photosynthetic parameters. Future applications should propagate uncertainty from a broader range of parameters, particularly soil hydraulic properties, rooting characteristics, and canopy processes. More efficient multi-objective calibration and inversion approaches (Denager et al., 2023; Bell et al., 2025) could further improve both parameter identifiability and robustness. An additional source of uncertainty arises from the representation of mixed cropping systems. At Qvidja, the forage grass and legume species are represented as a single effectively homogeneous canopy, although individual species may differ in hydraulic traits, stomatal regulation, and drought response. Resolving such within-canopy hydraulic heterogeneity would therefore be a valuable direction for future development.

Despite these uncertainties, the strong influence of plant hydraulics on crop productivity, water use, and drought responses demonstrated here highlights the value of explicitly representing hydraulic processes in crop models. SPY-C also reproduced net ecosystem exchange reasonably well at the study sites (Fig. S12), suggesting potential for applications in monitoring, reporting, and verification (MRV) of agricultural carbon balances (Smith et al., 2020; Guan et al., 2023; Wijmer et al., 2024). Developing SPY-C toward a robust MRV tool will nevertheless require a more complete representation of management and nutrient constraints. In particular, improved descriptions of sowing, harvesting, fertilization, and crop rotation, together with coupling of nitrogen dynamics to the carbon and water cycles (e.g. Stocker and Prentice, 2024), would allow crop growth and carbon–water exchange to respond more realistically to management. Combined with improved canopy, root, and parameter-inference schemes, these developments would strengthen the transferability of SPY-C across crop types, sites, and management regimes.

5 Conclusions

We examined the apparent hydraulic traits of typical annual and perennial boreal crops and their impact on crop productivity, water use efficiency, and drought response by combining multi-year carbon and water flux measurements from two Finnish crop fields with the newly developed model framework SPY-C, which explicitly couples plant hydraulic, photosynthesis, and soil moisture dynamics. SPY-C reproduced the observed carbon and water fluxes well enough to support field-scale inference of apparent hydraulic traits. Both oats and the perennial forage grass mixture exhibited relatively low apparent hydraulic efficiency and conservative hydraulic strategies, which are crucial for reducing rapid soil-water depletion and partly buffered crop functioning against atmospheric drought, thereby promoting drought avoidance and productivity under boreal conditions. Here,

we present SPY-C as an efficient tool for inferring apparent hydraulic traits and assessing their effects on crop performance across contrasting pedoclimate conditions. This can be fundamental for selecting and developing better crops and managements to support climate-smart and sustainable agriculture. We also underscore the good potential of SPY-C for broader applications in agricultural carbon monitoring, reporting, and verification to enhance the accuracy and predictive power in both current and future boreal climates.

Code and data availability. The meteorological and Sentinel-2 LAI data for Qvidja and Hauho sites are available from the Field Observatory website (https://www.fieldobservatory.org/) or from the Field Observatory dynamic data storage (Nevalainen et al., 2022b). The codes to retrieve Sentinel-2 satellite data and to calculate the leaf area index (LAI) are available from the Python satellitetools package (https://doi.org/10.5281/zenodo.5993291). Data for the gap-filled eddy covariance measurements are available at https://doi.org/10.57707/fmi-b2share.353cc686b81449d69117df30aeb3613c. The SPY-C model version used in this study is available at https://github.com/huitang-earth/SVMC/tree/v1.0.0. The model input and output are available at https://doi.org/10.57707/fmi-b2share.7536bc09eed44c71a08e87e545bc9406.

Author contributions. HT, SL, JV, LK, TP, JL designed the research. LK, HA, ON, MK, HV, JL collected observation data. HT, SL, JV, TP, IF, JPN, JL developed the SPY-C model. HT performed the research and data analysis. All the authors contribute to interpreting the results and writing the manuscript.

Competing interests. All authors declare no conflict of interest.

Acknowledgements. We thank Maria Tenkanen for helping improve the figures, Quentin Bell for inspiration about the model name and language checking, Laura Heimsch and Layla Höckerstedt for providing information of the study sites, Olli Niemitalo, Samu Varjonen and Iivari Kunttu for helpful discussions on the development of SPY-C. The authors wish to acknowledge CSC – IT Center for Science, Finland, for computational resources. ERA5-Land was downloaded from the Copernicus Climate Change Service (C3S). Neither the European Commission nor ECMWF is responsible for any use that may be made of the Copernicus information or data it contains.

Financial support. This work was supported by the Research Council of Finland (grant nos. 353073, 359342, 359533, 356138), the Strategic Research Council at the Research Council of Finland (grant no. 352431, 358257), the Ministry of Agriculture and Forestry of Finland (grant nos. VN/5094/2021 and VN/27979/2021), Business Finland (project 8391/31/2021), European Research Executive Agency (REA) through the Mission Soil project MARVIC (Grant Agreement: 101112942), Lantmännen Research Foundation and Lantmännen Group in Finland. In addition, this project has received funding from EU Horizon 2020 (grant no. 101056921).

References

Alves, RDFB., Menezes-Silva, PE., Loram-Lourenço, L., Abreu, IMPG., Alencar, KM., Sousa, LF., Almeida, SES., Aun, MA., Silva, MLF., Vasconcelos-Filho, SC., Silva, FG., Sales, JF., and Farnese, FS.: Exploring the Coordinated Hydraulic Plasticity across Organs in Soybean Plants Exposed to Drought Cycles, Environmental and Experimental Botany, 226, 105 871, https://doi.org/10.1016/j.envexpbot.2024.105871, 2024.

Anderegg, W. R. L., Klein, T., Bartlett, M., Sack, L., Pellegrini, A. F. A., Choat, B., and Jansen, S.: Meta-Analysis Reveals That Hydraulic Traits Explain Cross-Species Patterns of Drought-Induced Tree Mortality across the Globe, Proceedings of the National Academy of Sciences of the United States of America, 113, 5024–5029, https://doi.org/10.1073/pnas.1525678113, 2016.

Anderegg, W. R. L., Konings, A. G., Trugman, A. T., Yu, K., Bowling, D. R., Gabbitas, R., Karp, D. S., Pacala, S., Sperry, J. S., Sulman, B. N., and Zenes, N.: Hydraulic Diversity of Forests Regulates Ecosystem Resilience during Drought, Nature, 561, 538–541, https://doi.org/10.1038/s41586-018-0539-7, 2018.

Atkin, O. K., Bloomfield, K. J., Reich, P. B., Tjoelker, M. G., Asner, G. P., Bonal, D., Bönisch, G., Bradford, M. G., Cernusak, L. A., Cosio, E. G., Creek, D., Crous, K. Y., Domingues, T. F., Dukes, J. S., Egerton, J. J. G., Evans, J. R., Farquhar, G. D., Fyllas, N. M., Gauthier, P. P. G., Gloor, E., Gimeno, T. E., Griffin, K. L., Guerrieri, R., Heskel, M. A., Huntingford, C., Ishida, F. Y., Kattge, J., Lambers, H., Liddell, M. J., Lloyd, J., Lusk, C. H., Martin, R. E., Maksimov, A. P., Maximov, T. C., Malhi, Y., Medlyn, B. E., Meir, P., Mercado, L. M., Mirotchnick, N., Ng, D., Niinemets, Ü., O'Sullivan, O. S., Phillips, O. L., Poorter, L., Poot, P., Prentice, I. C., Salinas, N., Rowland, L. M., Ryan, M. G., Sitch, S., Slot, M., Smith, N. G., Turnbull, M. H., VanderWel, M. C., Valladares, F., Veneklaas, E. J., Weerasinghe, L. K., Wirth, C., Wright, I. J., Wythers, K. R., Xiang, J., Xiang, S., and Zaragoza-Castells, J.: Global Variability in Leaf Respiration in Relation to Climate, Plant Functional Types and Leaf Traits, New Phytologist, 206, 614–636, https://doi.org/10.1111/nph.13253, 2015.

Bell, Q., Gerin, S., Douglas, N., Quaife, T., Liski, J., and Viskari, T.: Calibrating Primary Crop Parameters to Capture Undersown Species Impacts, European Journal of Agronomy, 169, 127 676, https://doi.org/10.1016/j.eja.2025.127676, 2025.

Campolongo, F., Cariboni, J., and Saltelli, A.: An Effective Screening Design for Sensitivity Analysis of Large Models, Environmental Modelling & Software, 22, 1509–1518, https://doi.org/10.1016/j.envsoft.2006.10.004, 2007.

Canales, F. J., Rispail, N., García-Tejera, O., Arbona, V., Pérez-de-Luque, A., and Prats, E.: Drought Resistance in Oat Involves ABA-mediated Modulation of Transpiration and Root Hydraulic Conductivity, Environmental and Experimental Botany, 182, 104 333, https://doi.org/10.1016/j.envexpbot.2020.104333, 2021.

Cardoso, A. A., Andrade, M. T., Bucior, E. R., and Martins, S. C. V.: Plant Hydraulic Traits Influencing Crop Production in Water-Limited Environments, Plant Physiology, 199, https://doi.org/10.1093/plphys/kiaf521, 2025.

Choat, B., Jansen, S., Brodribb, T. J., Cochard, H., Delzon, S., Bhaskar, R., Bucci, S. J., Feild, T. S., Gleason, S. M., Hacke, U. G., Jacobsen, A. L., Lens, F., Maherali, H., Martínez-Vilalta, J., Mayr, S., Mencuccini, M., Mitchell, P. J., Nardini, A., Pittermann, J., Pratt, R. B., Sperry, J. S., Westoby, M., Wright, I. J., and Zanne, A. E.: Global Convergence in the Vulnerability of Forests to Drought, Nature, 491, 752–755, https://doi.org/10.1038/nature11688, 2012.

Corso, D., Delzon, S., Lamarque, L. J., Cochard, H., Torres-Ruiz, J. M., King, A., and Brodribb, T.: Neither Xylem Collapse, Cavitation, or Changing Leaf Conductance Drive Stomatal Closure in Wheat, Plant, Cell & Environment, 43, 854–865, https://doi.org/10.1111/pce.13722, 2020.

Denager, T., Sonnenborg, T. O., Looms, M. C., Bogena, H., and Jensen, K. H.: Point-Scale Multi-Objective Calibration of the Community Land Model (Version 5.0) Using in Situ Observations of Water and Energy Fluxes and Variables, Hydrology and Earth System Sciences, 27, 2827–2845, https://doi.org/10.5194/hess-27-2827-2023, 2023.

Drake, P. L., Veneklaas, E. J., Smith, N. G., Driever, S. M., and de Boer, H. J.: Temperature Acclimation of Chlorophyll Fluorescence and Carboxylation Capacity From Near-Instantaneous to Weekly Time Scales, Plant, Cell & Environment, 49, 5497–5510, https://doi.org/10.1111/pce.70555, 2026.

Fu, Z., Ciais, P., Wigneron, J.-P., Gentine, P., Feldman, A. F., Makowski, D., Viovy, N., Kemanian, A. R., Goll, D. S., Stoy, P. C., Prentice, I. C., Yakir, D., Liu, L., Ma, H., Li, X., Huang, Y., Yu, K., Zhu, P., Li, X., Zhu, Z., Lian, J., and Smith, W. K.: Global Critical Soil Moisture Thresholds of Plant Water Stress, Nature Communications, 15, 4826, https://doi.org/10.1038/s41467-024-49244-7, 2024.

Gan, Y., Duan, Q., Gong, W., Tong, C., Sun, Y., Chu, W., Ye, A., Miao, C., and Di, Z.: A Comprehensive Evaluation of Various Sensitivity Analysis Methods: A Case Study with a Hydrological Model, Environmental Modelling & Software, 51, 269–285, https://doi.org/10.1016/j.envsoft.2013.09.031, 2014.

Gerin, S., Vekuri, H., Liimatainen, M., Tuovinen, J.-P., Kekkonen, J., Kulmala, L., Laurila, T., Linkosalmi, M., Liski, J., Joki-Tokola, E., and Lohila, A.: Two Contrasting Years of Continuous N2O and CO2 Fluxes on a Shallow-Peated Drained Agricultural Boreal Peatland, Agricultural and Forest Meteorology, 341, 109 630, https://doi.org/10.1016/j.agrformet.2023.109630, 2023.

Gleason, S. M., Westoby, M., Jansen, S., Choat, B., Hacke, U. G., Pratt, R. B., Bhaskar, R., Brodribb, T. J., Bucci, S. J., Cao, K.-F., Cochard, H., Delzon, S., Domec, J.-C., Fan, Z.-X., Feild, T. S., Jacobsen, A. L., Johnson, D. M., Lens, F., Maherali, H., Martínez-Vilalta, J., Mayr, S., McCulloh, K. A., Mencuccini, M., Mitchell, P. J., Morris, H., Nardini, A., Pittermann, J., Plavcová, L., Schreiber, S. G., Sperry, J. S., Wright, I. J., and Zanne, A. E.: Weak Tradeoff between Xylem Safety and Xylem-Specific Hydraulic Efficiency across the World's Woody Plant Species, New Phytologist, 209, 123–136, https://doi.org/10.1111/nph.13646, 2016.

Gleason, S. M., Nalezny, L., Hunter, C., Bensen, R., Chintamanani, S., and Comas, L. H.: Growth and Grain Yield of Eight Maize Hybrids Are Aligned with Water Transport, Stomatal Conductance, and Photosynthesis in a Semi-Arid Irrigated System, Physiologia Plantarum, 172, 1941–1949, https://doi.org/10.1111/ppl.13400, 2021.

Gleason, S. M., Barnard, D. M., Green, T. R., Mackay, S., Wang, D. R., Ainsworth, E. A., Altenhofen, J., Brodribb, T. J., Cochard, H., Comas, L. H., Cooper, M., Creek, D., DeJonge, K. C., Delzon, S., Fritschi, F. B., Hammer, G., Hunter, C., Lombardozzi, D., Messina, C. D., Ocheltree, T., Stevens, B. M., Stewart, J. J., Vadez, V., Wenz, J., Wright, I. J., Yemoto, K., and Zhang, H.: Physiological Trait Networks Enhance Understanding of Crop Growth and Water Use in Contrasting Environments, Plant, Cell & Environment, 45, 2554–2572, https://doi.org/10.1111/pce.14382, 2022.

Guan, K., Jin, Z., Peng, B., Tang, J., DeLucia, E. H., West, P. C., Jiang, C., Wang, S., Kim, T., Zhou, W., Griffis, T., Liu, L., Yang, W. H., Qin, Z., Yang, Q., Margenot, A., Stuchiner, E. R., Kumar, V., Bernacchi, C., Coppess, J., Novick, K. A., Gerber, J., Jahn, M., Khanna, M., Lee, D., Chen, Z., and Yang, S.-J.: A Scalable Framework for Quantifying Field-Level Agricultural Carbon Outcomes, Earth-Science Reviews, 243, 104 462, https://doi.org/10.1016/j.earscirev.2023.104462, 2023.

Haddix, M. L., Gregorich, E. G., Helgason, B. L., Janzen, H., Ellert, B. H., and Francesca Cotrufo, M.: Climate, Carbon Content, and Soil Texture Control the Independent Formation and Persistence of Particulate and Mineral-Associated Organic Matter in Soil, Geoderma, 363, 114 160, https://doi.org/10.1016/j.geoderma.2019.114160, 2020.

Haugum, S. V., Thorvaldsen, P., Vandvik, V., and Velle, L. G.: Coastal Heathland Vegetation Is Surprisingly Resistant to Experimental Drought across Successional Stages and Latitude, Oikos, 130, 2015–2027, https://doi.org/10.1111/oik.08098, 2021.

Heckwolf, S., Heckwolf, M., Kaeppler, S. M., de Leon, N., and Spalding, E. P.: Image Analysis of Anatomical Traits in Stalk Transections of Maize and Other Grasses, Plant Methods, 11, 26, https://doi.org/10.1186/s13007-015-0070-x, 2015.

Heimsch, L., Lohila, A., Tuovinen, J.-P., Vekuri, H., Heinonsalo, J., Nevalainen, O., Korkiakoski, M., Liski, J., Laurila, T., and Kulmala, L.: Carbon Dioxide Fluxes and Carbon Balance of an Agricultural Grassland in Southern Finland, Biogeosciences, 18, 3467–3483, https://doi.org/10.5194/bg-18-3467-2021, 2021.

Heimsch, L., Vira, J., Fer, I., Vekuri, H., Tuovinen, J.-P., Lohila, A., Liski, J., and Kulmala, L.: Impact of Weather and Management Practices on Greenhouse Gas Flux Dynamics on an Agricultural Grassland in Southern Finland, Agriculture, Ecosystems & Environment, 374, 109 179, https://doi.org/10.1016/j.agee.2024.109179, 2024.

Henry, C., John, G. P., Pan, R., Bartlett, M. K., Fletcher, L. R., Scoffoni, C., and Sack, L.: A Stomatal Safety-Efficiency Trade-off Constrains Responses to Leaf Dehydration, Nature Communications, 10, 3398, https://doi.org/10.1038/s41467-019-11006-1, 2019.

Herman, J. and Usher, W.: SALib: An Open-Source Python Library for Sensitivity Analysis, Journal of Open Source Software, 2, 97, https://doi.org/10.21105/joss.00097, 2017.

Holloway-Phillips, M.-M. and Brodribb, T. J.: Contrasting Hydraulic Regulation in Closely Related Forage Grasses: Implications for Plant Water Use, Functional Plant Biology, 38, 594–605, https://doi.org/10.1071/FP11029, 2011a.

Holloway-Phillips, M.-M. and Brodribb, T. J.: Minimum Hydraulic Safety Leads to Maximum Water-Use Efficiency in a Forage Grass, Plant, Cell & Environment, 34, 302–313, https://doi.org/10.1111/j.1365-3040.2010.02244.x, 2011b.

Hu, L., Wu, M., Ju, W., Xing, X., Chen, J. M., and Zhu, H.: Improved Simulation of Gross Primary Production and Evapotranspiration in a Drought-Prone Temperate Deciduous Forest with *the BEPS-EcoHydro*, Agricultural and Forest Meteorology, 379, 111 031, https://doi.org/10.1016/j.agrformet.2026.111031, 2026.

Huo, J., Shi, Y., Chen, J., Zhang, H., Feng, L., Zhao, Y., and Zhang, Z.: Hydraulic Trade-off and Coordination Strategies Mediated by Leaf Functional Traits of Desert Shrubs, Frontiers in Plant Science, 13, https://doi.org/10.3389/fpls.2022.938758, 2022.

Jacob, V., Choat, B., Churchill, A. C., Zhang, H., Barton, C. V. M., Krishnananthaselvan, A., Post, A. K., Power, S. A., Medlyn, B. E., and Tissue, D. T.: High Safety Margins to Drought-Induced Hydraulic Failure Found in Five Pasture Grasses, Plant, Cell & Environment, 45, 1631–1646, https://doi.org/10.1111/pce.14318, 2022.

Joshi, J., Stocker, B. D., Hofhansl, F., Zhou, S., Dieckmann, U., and Prentice, I. C.: Towards a Unified Theory of Plant Photosynthesis and Hydraulics, Nature Plants, 8, 1304–1316, https://doi.org/10.1038/s41477-022-01244-5, 2022.

Kennedy, D., Swenson, S., Oleson, K. W., Lawrence, D. M., Fisher, R., Lola da Costa, A. C., and Gentine, P.: Implementing Plant Hydraulics in the Community Land Model, Version 5, Journal of Advances in Modeling Earth Systems, 11, 485–513, https://doi.org/10.1029/2018MS001500, 2019.

Kubota, S., Nishida, K., and Yoshida, S.: A Soil–Plant–Atmosphere Continuum Model Reflecting the Responses of Plant Hydraulic Resistance to Waterlogging, Journal of Hydrology, 672, 135 402, https://doi.org/10.1016/j.jhydrol.2026.135402, 2026.

Lamarque, L. J., Delzon, S., Toups, H., Gravel, A.-I., Corso, D., Badel, E., Burlett, R., Charrier, G., Cochard, H., Jansen, S., King, A., Torres-Ruiz, J. M., Pouzoulet, J., Cramer, G. R., Thompson, A. J., and Gambetta, G. A.: Over-Accumulation of Abscisic Acid in Transgenic Tomato Plants Increases the Risk of Hydraulic Failure, Plant, Cell & Environment, 43, 548–562, https://doi.org/10.1111/pce.13703, 2020.

Lamy, J.-B., Delzon, S., Bouche, P. S., Alia, R., Vendramin, G. G., Cochard, H., and Plomion, C.: Limited Genetic Variability and Phenotypic Plasticity Detected for Cavitation Resistance in a Mediterranean Pine, New Phytologist, 201, 874–886, https://doi.org/10.1111/nph.12556, 2014.

Launiainen, S., Guan, M., Salmivaara, A., and Kieloaho, A.-J.: Modeling Boreal Forest Evapotranspiration and Water Balance at Stand and Catchment Scales: A Spatial Approach, Hydrology and Earth System Sciences, 23, 3457–3480, https://doi.org/10.5194/hess-23-3457-2019, 2019.

Launiainen, S., Kieloaho, A.-J., Lindroos, A.-J., Salmivaara, A., Ilvesniemi, H., and Heiskanen, J.: Water Retention Characteristics of Mineral Forest Soils in Finland: Impacts for Modeling Soil Moisture, Forests, 13, 1797, https://doi.org/10.3390/f13111797, 2022.

Leakey, A. D. B., Ferguson, J. N., Pignon, C. P., Wu, A., Jin, Z., Hammer, G. L., and Lobell, D. B.: Water Use Efficiency as a Constraint and Target for Improving the Resilience and Productivity of C3 and C4 Crops, Annual Review of Plant Biology, 70, 781–808, https://doi.org/10.1146/annurev-arplant-042817-040305, 2019.

Li, S., Wang, J., Lu, S., Salmon, Y., Liu, P., and Guo, J.: Trade-Off between Hydraulic Safety and Efficiency in Plant Xylem and Its Influencing Factors, Forests, 14, 1817, https://doi.org/10.3390/f14091817, 2023.

Liu, H., Taylor, S. H., Xu, Q., Lin, Y., Hou, H., Wu, G., and Ye, Q.: Life History Is a Key Factor Explaining Functional Trait Diversity among Subtropical Grasses, and Its Influence Differs between C3 and C4 Species, Journal of Experimental Botany, 70, 1567–1580, https://doi.org/10.1093/jxb/ery462, 2019.

Liu, H., Ye, Q., Gleason, S. M., He, P., and Yin, D.: Weak Tradeoff between Xylem Hydraulic Efficiency and Safety: Climatic Seasonality Matters, New Phytologist, 229, 1440–1452, https://doi.org/10.1111/nph.16940, 2021a.

Liu, Y., Kumar, M., Katul, G. G., Feng, X., and Konings, A. G.: Plant Hydraulics Accentuates the Effect of Atmospheric Moisture Stress on Transpiration, Nature Climate Change, 10, 691–695, https://doi.org/10.1038/s41558-020-0781-5, 2020.

Liu, Y., Holtzman, N. M., and Konings, A. G.: Global Ecosystem-Scale Plant Hydraulic Traits Retrieved Using Model–Data Fusion, Hydrology and Earth System Sciences, 25, 2399–2417, https://doi.org/10.5194/hess-25-2399-2021, 2021b.

Lloyd, J. and Taylor, J. A.: On the Temperature Dependence of Soil Respiration, Functional Ecology, 8, 315–323, https://doi.org/10.2307/2389824, 1994.

Lu, Y., Sloan, B., Thompson, S. E., Konings, A. G., Bohrer, G., Matheny, A., and Feng, X.: Intra-Specific Variability in Plant Hydraulic Parameters Inferred From Model Inversion of Sap Flux Data, Journal of Geophysical Research: Biogeosciences, 127, e2021JG006 777, https://doi.org/10.1029/2021JG006777, 2022.

Martin-StPaul, N., Delzon, S., and Cochard, H.: Plant Resistance to Drought Depends on Timely Stomatal Closure, Ecology Letters, 20, 1437–1447, https://doi.org/10.1111/ele.12851, 2017.

Matzner, S. L., Rettedal, D. D., Harmon, D. A., and Beukelman, M. R.: Constraints to Hydraulic Acclimation under Reduced Light in Two Contrasting Phaseolus Vulgaris Cultivars, Journal of Experimental Botany, 65, 4409–4418, https://doi.org/10.1093/jxb/eru212, 2014.

Mirabel, A., Girardin, M. P., Metsaranta, J., Way, D., and Reich, P. B.: Increasing Atmospheric Dryness Reduces Boreal Forest Tree Growth, Nature Communications, 14, 6901, https://doi.org/10.1038/s41467-023-42466-1, 2023.

Morales, J. L. and Nocedal, J.: Remark on "Algorithm 778: L-BFGS-B: Fortran Subroutines for Large-Scale Bound Constrained Optimization", ACM Trans. Math. Softw., 38, 7:1–7:4, https://doi.org/10.1145/2049662.2049669, 2011.

Morris, M. D.: Factorial Sampling Plans for Preliminary Computational Experiments, Technometrics, 33, 161–174, https://doi.org/10.1080/00401706.1991.10484804, 1991.

Muñoz-Sabater, J., Dutra, E., Agustí-Panareda, A., Albergel, C., Arduini, G., Balsamo, G., Boussetta, S., Choulga, M., Harrigan, S., Hersbach, H., Martens, B., Miralles, D. G., Piles, M., Rodríguez-Fernández, N. J., Zsoter, E., Buontempo, C., and Thépaut, J.-N.: ERA5-Land: A State-of-the-Art Global Reanalysis Dataset for Land Applications, Earth System Science Data, 13, 4349–4383, https://doi.org/10.5194/essd-13-4349-2021, 2021.

Nevalainen, O., Niemitalo, O., Fer, I., Juntunen, A., Mattila, T., Koskela, O., Kukkamäki, J., Höckerstedt, L., Mäkelä, L., Jarva, P., Heimsch, L., Vekuri, H., Kulmala, L., Stam, Å., Kuusela, O., Gerin, S., Viskari, T., Vira, J., Hyväluoma, J., Tuovinen, J.-P., Lohila, A., Laurila, T., Heinonsalo, J., Aalto, T., Kunttu, I., and Liski, J.: Towards Agricultural Soil Carbon Monitoring, Reporting, and Verification through the Field Observatory Network (FiON), Geoscientific Instrumentation, Methods and Data Systems, 11, 93–109, https://doi.org/10.5194/gi-11-93-2022, 2022a.

Nevalainen, O., Niemitalo, O., Fer, I., Juntunen, A., Mattila, T., Koskela, O., Kukkamäki, J., Höckerstedt, L., Mäkelä, L., Jarva, P., Heimsch, L., Vekuri, H., Kulmala, L., Stam, Å., Kuusela, O., Gerin, S., Viskari, T., Vira, J., Hyväluoma, J., Tuovinen, J.-P., Lohila, A., Laurila, T., Heinonsalo, J., Aalto, T., Kunttu, I., and Liski, J.: Field Observatory Dynamic Data Storage, https://doi.org/10.23728/fmi-b2share.56513f096ca442b19abdef30f63644ed, 2022b.

Ocheltree, T. W., Nippert, J. B., and Prasad, P. V. V.: A Safety vs Efficiency Trade-off Identified in the Hydraulic Pathway of Grass Leaves Is Decoupled from Photosynthesis, Stomatal Conductance and Precipitation, New Phytologist, 210, 97–107, https://doi.org/10.1111/nph.13781, 2016.

Palosuo, T., Heikkinen, J., and Regina, K.: Method for Estimating Soil Carbon Stock Changes in Finnish Mineral Cropland and Grassland Soils, Carbon Management, 6, 207–220, https://doi.org/10.1080/17583004.2015.1131383, 2015.

Pereira, T. S., Oliveira, L. A., Andrade, M. T., Haverroth, E. J., Cardoso, A. A., and Martins, S. C. V.: Linking Water-Use Strategies with Drought Resistance across Herbaceous Crops, Physiologia Plantarum, 176, e14 114, https://doi.org/10.1111/ppl.14114, 2024.

Poque, S., Carlson-Nilsson, U., Omer, M., Himanen, K., and Khazaei, H.: Exploring an Automated Indoor High-Throughput Phenotyping Facility to Investigate the Response of Faba Bean to Water Stress, https://doi.org/10.21203/rs.3.rs-6461902/v1, 2025.

Pritzkow, C., Williamson, V., Szota, C., Trouvé, R., and Arndt, S. K.: Phenotypic Plasticity and Genetic Adaptation of Functional Traits Influences Intra-Specific Variation in Hydraulic Efficiency and Safety, Tree Physiology, 40, 215–229, https://doi.org/10.1093/treephys/tpz121, 2020.

Qiao, S., Wang, H., Prentice, I. C., and Harrison, S. P.: Optimality-Based Modelling of Climate Impacts on Global Potential Wheat Yield, Environmental Research Letters, 16, 114 013, https://doi.org/10.1088/1748-9326/ac2e38, 2021.

Ramírez-Valiente, J. A., Poyatos, R., Blackman, C. J., Cabon, A., Castells, E., Cochard, H., Creek, D., Delzon, S., García-Valdés, R., Limousin, J.-M., López, R., Martin-StPaul, N., Moreno, M., Rowland, L., Santiago, L. S., Schuldt, B., Torres-Ruiz, J. M., Valade, A., Martínez-Vilalta, J., and Mencuccini, M.: Limited Plastic Responses in Safety Traits Support Greater Hydraulic Risk under Drier Conditions, Nature Ecology & Evolution, pp. 1–12, https://doi.org/10.1038/s41559-025-02830-4, 2025.

Rantanen, M., Kämäräinen, M., Niittynen, P., Phoenix, G. K., Lenoir, J., Maclean, I., Luoto, M., and Aalto, J.: Bioclimatic Atlas of the Terrestrial Arctic, Scientific Data, 10, 40, https://doi.org/10.1038/s41597-023-01959-w, 2023.

Reichstein, M., Falge, E., Baldocchi, D., Papale, D., Aubinet, M., Berbigier, P., Bernhofer, C., Buchmann, N., Gilmanov, T., Granier, A., Grünwald, T., Havránková, K., Ilvesniemi, H., Janous, D., Knohl, A., Laurila, T., Lohila, A., Loustau, D., Matteucci, G., Meyers, T., Miglietta, F., Ourcival, J.-M., Pumpanen, J., Rambal, S., Rotenberg, E., Sanz, M., Tenhunen, J., Seufert, G., Vaccari, F., Vesala, T., Yakir, D., and Valentini, R.: On the Separation of Net Ecosystem Exchange into Assimilation and Ecosystem Respiration: Review and Improved Algorithm, Global Change Biology, 11, 1424–1439, https://doi.org/10.1111/j.1365-2486.2005.001002.x, 2005.

Roitsch, T., Himanen, K., Chawade, A., Jaakola, L., Nehe, A., and Alexandersson, E.: Functional Phenomics for Improved Climate Resilience in Nordic Agriculture, Journal of Experimental Botany, 73, 5111–5127, https://doi.org/10.1093/jxb/erac246, 2022.

Sanchez-Martinez, P., Martínez-Vilalta, J., Dexter, K. G., Segovia, R. A., and Mencuccini, M.: Adaptation and Coordinated Evolution of Plant Hydraulic Traits, Ecology Letters, 23, 1599–1610, https://doi.org/10.1111/ele.13584, 2020.

Schaap, M. G. and Van Genuchten, M. T.: A Modified Mualem–van Genuchten Formulation for Improved Description of the Hydraulic Conductivity Near Saturation, Vadose Zone Journal, 5, 27–34, https://doi.org/10.2136/vzj2005.0005, 2006.

Schell, V., Kervroëdan, L., Corso, D., N'do, D. Y., Faucon, M.-P., and Delzon, S.: Greater Resistance to Drought-Induced Embolism Is Linked to Higher Yield Maintenance in Soybean, Plant, Cell & Environment, https://doi.org/10.1111/pce.15538, 2025.

Seddon, A. W. R., Macias-Fauria, M., Long, P. R., Benz, D., and Willis, K. J.: Sensitivity of Global Terrestrial Ecosystems to Climate Variability, Nature, 531, 229–232, https://doi.org/10.1038/nature16986, 2016.

Sierra, C. A., Ceballos-Núñez, V., Hartmann, H., Herrera-Ramírez, D., and Metzler, H.: Ideas and Perspectives: Allocation of Carbon from Net Primary Production in Models Is Inconsistent with Observations of the Age of Respired Carbon, Biogeosciences, 19, 3727–3738, https://doi.org/10.5194/bg-19-3727-2022, 2022.

Smith, P., Soussana, J.-F., Angers, D., Schipper, L., Chenu, C., Rasse, D. P., Batjes, N. H., van Egmond, F., McNeill, S., Kuhnert, M., Arias-Navarro, C., Olesen, J. E., Chirinda, N., Fornara, D., Wollenberg, E., Álvaro-Fuentes, J., Sanz-Cobena, A., and Klumpp, K.: How to Measure, Report and Verify Soil Carbon Change to Realize the Potential of Soil Carbon Sequestration for Atmospheric Greenhouse Gas Removal, Global Change Biology, 26, 219–241, https://doi.org/10.1111/gcb.14815, 2020.

Sperry, J. S. and Love, D. M.: What Plant Hydraulics Can Tell Us about Responses to Climate-Change Droughts, New Phytologist, 207, 14–27, https://doi.org/10.1111/nph.13354, 2015.

Spinoni, J., Vogt, J. V., Naumann, G., Barbosa, P., and Dosio, A.: Will Drought Events Become More Frequent and Severe in Europe?, International Journal of Climatology, 38, 1718–1736, https://doi.org/10.1002/joc.5291, 2018.

Stocker, B. D. and Prentice, I. C.: CN-model: A Dynamic Model for the Coupled Carbon and Nitrogen Cycles in Terrestrial Ecosystems, https://doi.org/10.1101/2024.04.25.591063, 2024.

Sun, Q., Gilgen, A. K., Signarbieux, C., Klaus, V. H., and Buchmann, N.: Cropping Systems Alter Hydraulic Traits of Barley but Not Pea Grown in Mixture, Plant, Cell & Environment, 44, 2912–2924, https://doi.org/10.1111/pce.14054, 2021.

Torres-Ruiz, J. M., Cochard, H., Delzon, S., Boivin, T., Burlett, R., Cailleret, M., Corso, D., Delmas, C. E. L., De Caceres, M., Diaz-Espejo, A., Fernández-Conradi, P., Guillemot, J., Lamarque, L. J., Limousin, J.-M., Mantova, M., Mencuccini, M., Morin, X., Pimont, F., De Dios, V. R., Ruffault, J., Trueba, S., and Martin-StPaul, N. K.: Plant Hydraulics at the Heart of Plant, Crops and Ecosystem Functions in the Face of Climate Change, New Phytologist, 241, 984–999, https://doi.org/10.1111/nph.19463, 2024.

Vekuri, H., Tuovinen, J.-P., Kulmala, L., Papale, D., Kolari, P., Aurela, M., Laurila, T., Liski, J., and Lohila, A.: A Widely-Used Eddy Covariance Gap-Filling Method Creates Systematic Bias in Carbon Balance Estimates, Scientific Reports, 13, 1–9, https://doi.org/10.1038/s41598-023-28827-2, 2023.

Vico, G. and Brunsell, N. A.: Tradeoffs between Water Requirements and Yield Stability in Annual vs. Perennial Crops, Advances in Water Resources, 112, 189–202, https://doi.org/10.1016/j.advwatres.2017.12.014, 2018.

Vira, J., Vekuri, H., Nevalainen, O., Korkiakoski, M., Mattila, T., Aaltonen, H., Koskinen, M., Lohila, A., Pihlatie, M., and Liski, J.: Improving Agricultural Carbon Monitoring with Sentinel-2 and Eddy-Covariance-Based Plant Productivity Estimates, Carbon Management, 16, 2568 042, https://doi.org/10.1080/17583004.2025.2568042, 2025.

Viskari, T., Pusa, J., Fer, I., Repo, A., Vira, J., and Liski, J.: Calibrating the Soil Organic Carbon Model Yasso20 with Multiple Datasets, Geoscientific Model Development, 15, 1735–1752, https://doi.org/10.5194/gmd-15-1735-2022, 2022.

Wang, D. R., Venturas, M. D., Mackay, D. S., Hunsaker, D. J., Thorp, K. R., Gore, M. A., and Pauli, D.: Use of Hydraulic Traits for Modeling Genotype-specific Acclimation in Cotton under Drought, New Phytologist, 228, 898–909, https://doi.org/10.1111/nph.16751, 2020.

Weiss, M., Baret, F., and Jay, S.: S2 Toolbox Level 2 Product Algorithms, Tech. rep., European Space Agency, 2020.

Wijmer, T., Al Bitar, A., Arnaud, L., Fieuzal, R., and Ceschia, E.: AgriCarbon-EO v1.0.1: Large-Scale and High-Resolution Simulation of Carbon Fluxes by Assimilation of Sentinel-2 and Landsat-8 Reflectances Using a Bayesian Approach, Geoscientific Model Development, 17, 997–1021, https://doi.org/10.5194/gmd-17-997-2024, 2024.

Xia, J., Yuan, W., Wang, Y.-P., and Zhang, Q.: Adaptive Carbon Allocation by Plants Enhances the Terrestrial Carbon Sink, Scientific Reports, 7, 3341, https://doi.org/10.1038/s41598-017-03574-3, 2017.

Yao, G.-Q., Nie, Z.-F., Zeng, Y.-Y., Waseem, M., Hasan, M. M., Tian, X.-Q., Liao, Z.-Q., Siddique, K. H. M., and Fang, X.-W.: A Clear Trade-off between Leaf Hydraulic Efficiency and Safety in an Aridland Shrub during Regrowth, Plant, Cell & Environment, 44, 3347–3357, https://doi.org/10.1111/pce.14156, 2021.

Yu, L., Gao, X., and Zhao, X.: Global Synthesis of the Impact of Droughts on Crops' Water-Use Efficiency (WUE): Towards Both High WUE and Productivity, Agricultural Systems, 177, 102 723, https://doi.org/10.1016/j.agsy.2019.102723, 2020.

Zhao, Q., Chen, J., Kang, J., and Kang, S.: Trade-Offs Between Hydraulic Efficiency and Safety in Cotton (Gossypium Hirsutum L.) Stems Under Elevated CO2 and Salt Stress, Plants, 14, 298, https://doi.org/10.3390/plants14020298, 2025.